

Profile and polarization characteristics of energetic pulsars

Patrick Weltevrede and Simon Johnston

Australia Telescope National Facility, CSIRO, P.O. Box 76, Epping, NSW 1710, Australia.

25 October 2021

ABSTRACT

In this paper we compare the characteristics of pulsars with a high spin-down energy loss rate (\dot{E}) against those with a low \dot{E} . We show that the differences in the total intensity pulse morphology between the two classes are in general rather subtle. A much more significant difference is the fractional polarization which is very high for high \dot{E} pulsars and low for low \dot{E} pulsars. The \dot{E} at the transition is very similar to the death line predicted for curvature radiation. This suggests a possible link between high energy and radio emission in pulsars and could imply that γ -ray efficiency is correlated with the degree of linear polarization in the radio band. The degree of circular polarization is in general higher in the second component of doubles, which is possibly caused by the effect of co-rotation on the curvature of the field lines in the inertial observer frame.

The most direct link between the high energy emission and the radio emission could be the sub-group of pulsars which we call the energetic wide beam pulsars. These young pulsars have very wide profiles with steep edges and are likely to be emitted from a single magnetic pole. The similarities with the high energy profiles suggest that both types of emission are produced at the same extended height range in the magnetosphere. Alternatively, the beams of the energetic wide beam pulsars could be magnified by propagation effects in the magnetosphere. This would naturally lead to decoupling of the wave modes, which could explain the high degree of linear polarization. As part of this study, we have discovered three previous unknown interpulse pulsars (and we detected one for the first time at 20 cm). We also obtained rotation measures for 18 pulsars whose values had not previously been measured.

Key words: polarization — pulsars:general — pulsars: individual PSRs J0905–5127, J1126–6054, J1611–5209, J1637–4553 — radiation mechanisms: non-thermal

1 INTRODUCTION

Pulsars are observed to be spinning down with time. The spin-down energy loss rate \dot{E} , which is the loss of kinetic energy, is given by

$$\dot{E} = 4\pi^2 I \dot{P} P^{-3} \quad (1)$$

where I is the moment of inertia of the star (generally taken to be 10^{45} g cm²), P its spin period and \dot{P} its spin down rate. Some of the loss of spin-down energy emerges as radiation across the entire electromagnetic spectrum from radio to γ -rays. The radio emission accounts for only $\sim 10^{-6}$ of the energy budget (e.g. Lorimer & Kramer 2005) whereas up to a few percent is emitted in the γ -ray band (e.g. Thompson 2004), with the rest converted to magnetic dipole radiation and some form of pulsar wind.

It has been evident for more than a decade that pulsars with high \dot{E} have different polarization characteristics to those with lower \dot{E} . Many high \dot{E} pulsars are highly linearly polarized (e.g. Qiao et al. 1995; von Hoensbroech et al. 1998;

Crawford et al. 2001). The pulse profiles of high \dot{E} pulsars are believed to be generally simple, consisting of either one or two prominent components (e.g. Huguenin et al. 1971; Rankin 1983). Johnston & Weisberg (2006) found that, in the high \dot{E} pulsars with double profiles, the total power and the circular polarization usually dominates in the trailing component and that the swing of position angle (PA) of the linearly polarized radiation is steeper under the trailing component. They interpreted these results as showing that the beam of high \dot{E} pulsars consisted of a single conal ring at a relatively high height. Karastergiou & Johnston (2007) incorporated these results into their pulsar beam model. In their model, there is a sharp distinction between pulsars with $\dot{E} > 10^{35}$ erg s⁻¹ and those with smaller \dot{E} .

High \dot{E} pulsars are not only interesting because of their distinct properties in the radio band, but also because a subset of them emit pulsed high energy emission. There are three different families of high energy emission models in the literature which places the emitting regions at different locations in the pulsar magnetosphere. In the polar cap

models (e.g. Daugherty & Harding 1996) the emitting region is close to the neutron star surface, while outer gap models (e.g. Cheng et al. 1986) place the emitting region near the light cylinder. Finally, in slot gap models (e.g. Muslimov & Harding 2004a) the particle acceleration occurs in a region bordering the last open field lines. In the polar cap models the young pulsars are thought to produce pairs through curvature radiation (e.g. Harding & Muslimov 2001), while older pulsars produce pairs only through inverse-Compton scattering (e.g. Muslimov & Harding 2004b). In the outer gap model pairs are formed by the interaction of thermal X-ray photons from the neutron star surface with γ -ray photons (e.g. Romani 1996). All models have in common that high \dot{E} pulsars should be brighter γ -ray sources than low \dot{E} pulsars, something which is confirmed by EGRET (Thompson 2004).

We have recently embarked on a long-term timing campaign to monitor a large sample of young, high \dot{E} pulsars. The ephemerides obtained from timing will be used to provide accurate phase tagging of γ -ray photons obtained from the Fermi Gamma-Ray Space Telescope (formerly known as GLAST Smith et al. 2008) and AGILE (Pellizzoni et al. 2008) satellites, with the expectation that the number of γ -ray pulsars will increase from the current 7 to over 100 (Gonthier et al. 2007). Of the ~ 80 non millisecond pulsars in the pulsar catalogue maintained by the ATNF¹ (Manchester et al. 2005) with $\dot{E} > 10^{35}$ erg s⁻¹, we have obtained polarization profiles at 1.4 GHz for 61, a substantial increase in the number available to previous studies. In this paper, therefore, we examine the differences between high and low \dot{E} pulsars. In total, we use pulse profiles from 352 pulsars, which includes the 61 energetic pulsars and a comparison sample of intermediate and low \dot{E} pulsars in order to draw general conclusions about the pulsar population.

The paper is organized as follows. We start with explaining the details of the observations and the data analysis. In section 3 we then describe the polarization profiles of four pulsars for which we found an interpulse at 20 cm and present new rotation measures. In section 4 the total intensity profiles of the pulsars are discussed, followed by a discussion of the polarization properties. Finally we will discuss the results in section 6, followed by the conclusions. The polarization profiles of all the pulsars can be found in appendix A (those for which we have a 20 cm and a 10 cm profile) and appendix B (those for which we only have a 20 cm profile). The plots of the pulse profiles can also be found on the internet². Finally, a table with derived properties from the pulse profiles can be found in appendix C³. The appendices are only available in the on-line version of this publication.

2 OBSERVATIONS AND DATA ANALYSIS

The procedure to generate pulse profiles for the pulsars which are timed for the Fermi and AGILE satellites is com-

plicated by the fact that the pulse profiles of individual (short) observations have typically a low signal to noise ratio (S/N). It is therefore required to sum all the available observations in order to obtain a template profile with a higher S/N . This procedure is described in some detail in this section.

2.1 Observations

All the observations were made at the Parkes telescope in Australia using the centre beam of the 20 cm multibeam receiver (which has a bandwidth of 256 MHz and has a noise equivalent flux density of ~ 35 Jy on a cold sky) and the 10/50 cm receiver (which has at 10 cm a bandwidth of 1024 MHz and has a noise equivalent flux density of ~ 49 Jy on a cold sky). This paper will focus mainly on the 20 cm data, because that is wavelength at which the majority of observations were made. However for some highly scattered pulsars it is also useful to consider the 10 cm data. The 50 cm data is not used, because the profiles are scattered at that frequency in many cases. The timing program started in April 2007 and each pulsar is typically observed once per month at 20 cm and twice per year at 10 and 50 cm. The two polarization channels of the linear feeds of the receiver were converted into Stokes parameters, resampled and folded at the pulse period by a digital filterbank. In our case a pulse profile with 1024 bins and 1024 frequency channels was dumped every 30 seconds on hard disk. Before each observation a calibration signal, injected into the feed at a 45° angle to the probes, was recorded which is then used to determine the phase delay and relative gain between the two polarization channels.

The data were processed using the *PSRCHIVE* package (Hotan et al. 2004). The data of each observing session were first checked for narrow band radio frequency interference (RFI). An automatic procedure using the median smoothed difference of the bandpass, was used to identify the affected frequency channels in the calibration observations. The flagged channels were left out of all the observations of a particular observing day, making the automatic procedure more robust in finding weaker RFI which is not always identified. The remaining frequency channels were added together and the resulting sequence of profiles was then visually inspected for impulsive RFI. The sub-integrations in where RFI was particularly strong were left out of further data processing.

The 20 cm multibeam receiver has a significant cross-coupling between the two dipoles affecting the polarization of the pulsar signal. For instance, a highly linearly polarized signal induces artificial circular polarization. These effects are measured as a function of parallactic angle for PSR J0437-4715 for the Parkes Pulsar Timing Array project (Manchester et al. 2008, in preparation), which allows the construction of a polarimetric calibration model (van Straten 2004). We have applied this model to all the observations using the 20 cm multibeam receiver, which reduces the artifacts in the Stokes parameters considerably.

2.2 Summing of the individual observations

For some pulsars the timing noise is so severe that the pulse period predicted by the timing solution in the pulsar cat-

¹ <http://www.atnf.csiro.au/research/pulsar/psrcat>

² <http://www.atnf.csiro.au/people/joh414/ppdata/index.html>

³ This table is also available in electronic form at the CDS via anonymous ftp to cdsarc.u-strasbg.fr (130.79.128.5) or via <http://cdsweb.u-strasbg.fr/cgi-bin/qcat?J/MNRAS/>

ologue is not accurate enough to fold the data. In such a case the pulsar appears to drift in longitude in successive sub-integrations. We therefore applied the updated timing solutions to align the sub-integrations within individual observations.

To produce high S/N profiles the individual observations must be added together. Because many pulsars involved in this timing program have severe timing noise and show glitches, it is difficult to use the timing solution to add the observations together. Instead a scheme was followed in which the observations are correlated with each other in order to find the offsets in pulse longitude between the profiles. These offsets were applied directly to the individual observations using custom software in order to sum the profiles. The sum of the profiles (i.e. the standard or template) has a higher S/N than the individual profiles and can then be correlated with the individual observations to determine the offsets in pulse longitude with higher precision, hence making a more accurate standard. This procedure is repeated one more time to make the final pulse profile.

2.3 Faraday de-rotation

The interstellar medium interacts with the radio waves of pulsars, causing a number of frequency and time dependent effects. One of these effects is Faraday rotation, where the interstellar magnetic field component parallel to the line of sight causes a difference in the propagation speeds of the left- and right-hand circular polarization signal components. This effect causes the polarization vector to rotate in the Stokes Q and U plane and the angle is a function of frequency and the rotation measure (RM). It is therefore necessary to de-rotate Stokes Q and U before summing the frequency channels in an observation.

A similar procedure has to be followed when the profiles of different observations are summed together, because different frequency channels were flagged and deleted in different observations. This means that although the centre frequencies are identical for the different observations, their weighted mid-frequencies are slightly different. The *PSRCHIVE* package de-rotates Stokes Q and U with respect to this weighted mid-frequency of the band and therefore it is necessary to take the RM into account when profiles of different observations are summed together. This is done by rotating Stokes Q and U of each observation with respect to infinite frequency using custom software before adding individual observations together.

2.4 Making frequency standards

In order to be able to measure the RM for pulsars for which no sufficiently accurate values were available one needs to keep frequency resolution. This is done by summing the observations together using custom software which takes into account the pulse longitude offsets found by correlating the profiles of the individual observations (as described section 2.2). A complication is that *PSRCHIVE* de-disperses the data with respect to the non-weighted centre frequency of the band, while the pulse longitude offsets are determined using de-dispersed profiles with respect to the weighted mid-frequency. It is therefore necessary to include a dispersion

time delay corresponding with the difference in the weighted and non-weighted mid-frequency when the observations are added together.

3 RESULTS ON INDIVIDUAL PULSARS

3.1 Newly discovered interpsules

While analysing the data described in this paper we discovered four interpsules which have not been previously reported at 20 cm in the literature. The polarization profiles of these pulsars are shown in Fig. 1 and discussed in some detail below. In all cases there is no evidence that the interpulse only appears sporadically rather than be weakly present in all observations.

3.1.1 PSR J0905-5127

Profiles of this pulsar were presented first in D'Amico et al. (1998). In their figure, there appears to be little sign of the interpulse at 20 cm, with perhaps a hint at 70 cm. In our observations at 20 cm, the interpulse is very weak in comparison to the main pulse with an intensity ratio of ~ 17 . The separation between the centroid of the main and interpsules is 175° . The main pulse is a clear double with a total width of $\sim 20^\circ$ but not much structure can be discerned in the interpulse because of the low S/N , although its width appears to be narrower than that of the main pulse. The interpulse is separated by 180° from the trailing component of the main pulse, suggesting that the interpulse could be the trailing component of a double. The polarization swing across both the main and interpsules is rather flat, and we cannot attempt a rotating vector model fit (RVM; Radhakrishnan & Cooke 1969). We do not have sufficient S/N to make any claims about the interpulse at either 10 cm or 50 cm from our data.

3.1.2 PSR J1126-6054

The interpulse of PSR J1126-6054 is too weak to be seen in the profile presented in Johnston et al. (1992). However, it is just visible in our 20 cm data with a peak amplitude about one tenth of that of the main pulse. The peak-to-peak separation between the main and interpsules is $\sim 174^\circ$. This low \dot{E} pulsar has a low degree of linear polarization in its main pulse, which explains the absence of significant linear polarization in the much weaker interpulse. The interpulse appears to be significantly narrower, though the low S/N makes the width difficult to measure. At 50 cm, the interpulse is marginally stronger with respect to the main pulse whereas at 10 cm it is not detected.

3.1.3 PSR J1611-5209

There is no obvious interpulse at 20 cm in the profile presented in Johnston et al. (1992). However, Karastergiou et al. (2005) reported a low-amplitude interpulse in their 10 cm data. In our 20 cm data we clearly see the interpulse which has a peak amplitude less than 0.1 that of the main pulse. The separation between the main and interpulse is $\sim 177^\circ$. The main pulse has a total width of $\sim 10^\circ$

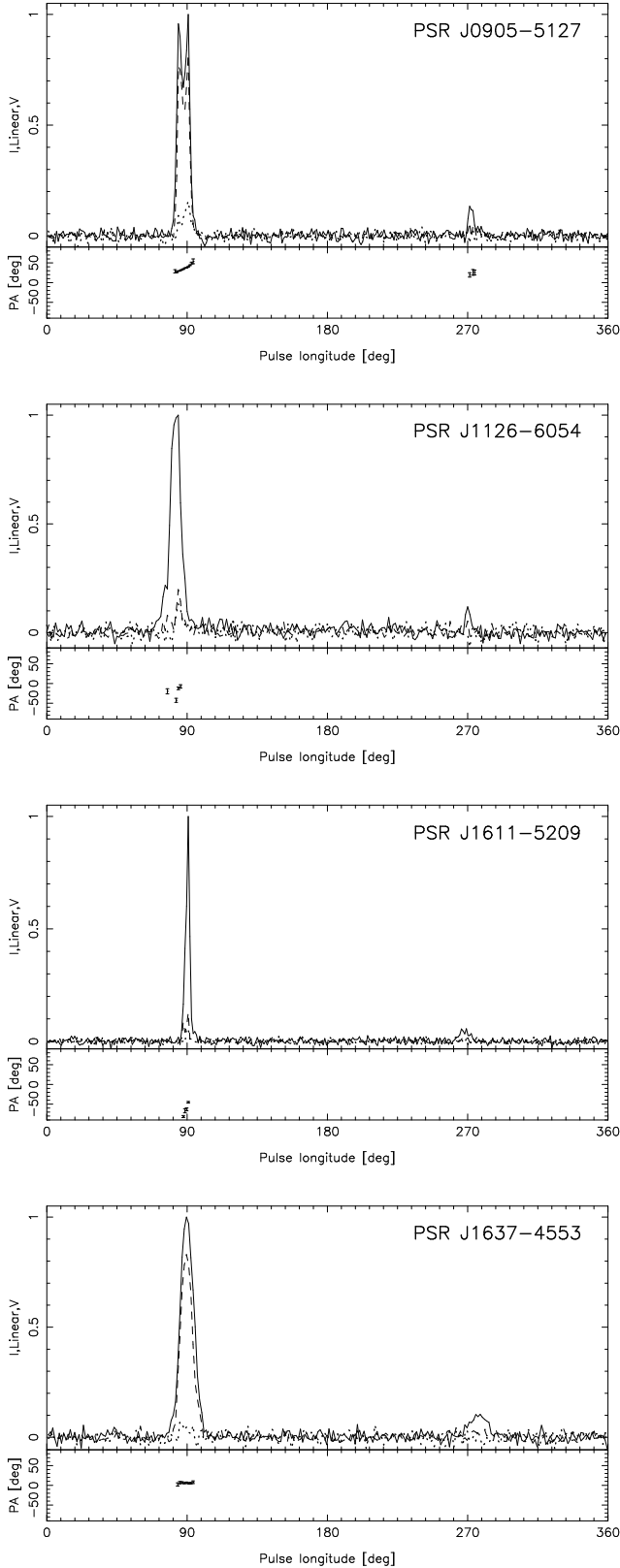


Figure 1. The pulse profile of the four pulsars for which we report an interpulse at an observing wavelength of 20 cm. The top panels show the total intensity profile (solid line), linear polarization (dashed line) and circular polarization (dotted line). The peak intensity of the profiles are normalized to one. The bottom panels show the PA of the linear polarization (for the pulse longitude bins in where the linear polarization was detected above 2σ).

Name	RM [rad m ⁻²]	l [deg]	b [deg]	DM [pc cm ⁻³]	d [kpc]
J1052-5954	-280 ± 24	288.55	-0.40	491	13.55
J1115-6052	257 ± 18	291.56	-0.13	228.2	6.76
J1156-5707	238 ± 19	295.45	4.95	243.5	20.40
J1524-5625	180 ± 20	323.00	0.35	152.7	3.84
J1524-5706	-470 ± 20	322.57	-0.19	833	21.59
J1638-4417	160 ± 25	339.77	1.73	436.0	8.46
J1702-4128	-160 ± 20	344.74	0.12	367.1	5.18
J1705-3950	-106 ± 14	346.34	0.72	207.1	3.86
J1737-3137	448 ± 17	356.74	0.15	488.2	5.88
J1738-2955	-200 ± 20	358.38	0.72	223.4	3.91
J1801-2154	160 ± 40	7.83	0.55	387.9	5.15
J1809-1917	41 ± 17	11.09	0.08	197.1	3.71
J1815-1738	175 ± 20	13.18	-0.27	728	9.06
J1828-1101	45 ± 20	20.49	0.04	607.4	7.26
J1837-0604	450 ± 25	25.96	0.26	462	6.19
J1841-0345	447 ± 15	28.42	0.44	194.32	4.15
J1845-0743	440 ± 12	25.43	-2.30	281.0	5.85
J1853-0004	647 ± 16	33.09	-0.47	438.2	6.58

Table 1. The pulsars for which new values of the RM were measured. From left to right the columns are the pulsar name, the measured rotation measures, the galactic longitude and latitude, the dispersion measure and the best available distance estimate.

and consists of at least two components with a low fractional polarization. The low S/N in the interpulse precludes any measurement of the polarization, but the overall width seems similar to main pulse.

3.1.4 PSR J1637-4553

This pulsar has a very weak interpulse (about one tenth in amplitude compared to the main pulse), which is perhaps just visible in the existing literature (Johnston et al. 1992). The separation between the main and interpulses is $\sim 173^\circ$, and although weak, the interpulse seems to be the same width as the $\sim 20^\circ$ of the main pulse. The polarization of the interpulse is hard to determine, although the main pulse is virtually 100% polarized. At 50 cm, the interpulse has the same separation from the main pulse and roughly the same relative amplitude as at 20 cm. Our low S/N at 10 cm makes the interpulse undetectable.

3.2 New rotation measures

As mentioned in section 2, the interstellar magnetic field parallel to the line of sight causes the polarization vector to rotate in the Stokes Q and U plane. In order to derive the degree of linear polarization it is therefore necessary to correct for this rotation before summing the frequency channels across the frequency band. The amount of rotation of the PA depend on the rotation measure RM and values for the RM were obtained from the pulsar catalogue. However, not all the pulsars have a published value for its RM (or one with sufficient accuracy). We therefore measured the RM for a number of objects in our sample.

The RM can be measured by fitting the change of the PA (ψ) across the frequency band with the Faraday rotation formula

\dot{E} [erg s $^{-1}$]	Single	Double	Multiple	Total
$10^{35} - 10^{38}$	27 (53%)	17 (33%)	7 (14%)	51
$10^{33} - 10^{35}$	53 (47%)	43 (38%)	16 (14%)	112
$10^{28} - 10^{33}$	52 (46%)	46 (40%)	16 (14%)	114

Table 2. The classification of the profiles for different \dot{E} bins. Pulsars with a $S/N < 30$ were excluded as well as the profiles marked to show substantial scattering.

$$\psi(\lambda) = \psi_{\infty} + RM\lambda^2, \quad (2)$$

where λ is the observing wavelength of the considered frequency channel and ψ_{∞} is the PA at infinite frequency. When different pulse longitude bins of the pulse profile show a similar frequency dependence of ψ one can be confident in the measured RM. The RM is obtained by calculating the weighted average of the fits of equation (2) for different bins in where there is enough linear polarization present. The new RM values are listed in Table 1. Only PSR J1809–1917 has a previously published RM which we include in the table because our value of 41 rad m $^{-2}$ differs significantly from the 130 rad m $^{-2}$ quoted by Han et al. (2006).

4 TOTAL INTENSITY PULSE PROFILES

In this and the following section we investigate if, and how, the beams of high \dot{E} pulsars differ from those of low \dot{E} pulsars. As we are going to investigate basic pulse profile properties in a statistical way, it is important to consider the effects of a low S/N and interstellar scattering. Because the high \dot{E} pulsars tend to be younger they have on average lower galactic latitude than older pulsars, hence they tend to be more affected by interstellar scattering. Therefore low S/N observations and profiles which are clearly affected by interstellar scattering were excluded from the statistics.

4.1 Pulse profile morphology

It has been pointed out by several authors (e.g. Huguenin et al. 1971; Rankin 1983; Johnston & Weisberg 2006; Karastergiou & Johnston 2007) that the profiles of high \dot{E} pulsars are relatively simple. A problem with measuring “profile complexity” is that it is not a well defined quantity, hence it is highly subjective. In order to make the results objective and better reproducible one should quantify the amount of complexity in a mathematical way. We will therefore explore ways to quantify different aspects of profile complexity, because it is difficult to come up with a definition which covers all facets of profile complexity. Only the total intensity (Stokes parameter I) profiles are considered in this section, while the polarization properties are investigated in the next section.

4.1.1 Profile classification

Pulse profiles are often described in terms of “components”, which are attributed to structure in the pulsar beam. There are different models in the literature describing the structure of the radio beam of pulsars. The beam could be composed out of a core and one or more cones (Rankin 1983),

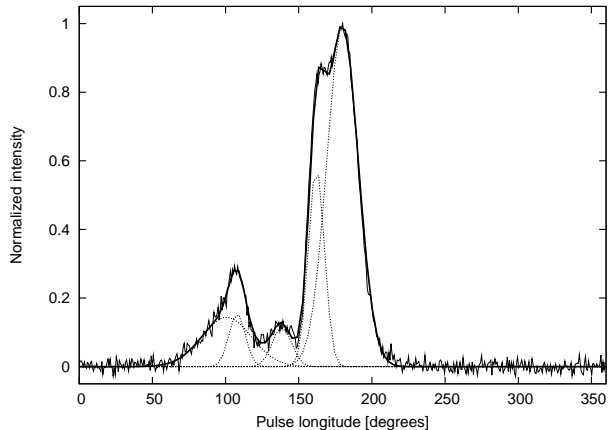


Figure 2. The decomposition of the pulse profile of PSR J1803–2137 at 20 cm into five von Mises functions (the dotted curves). The sum of these functions (the thick solid line) is a good representation of the observed pulse profile (thin solid line).

randomly distributed patches (Lyne & Manchester 1988) or patchy cones (Karastergiou & Johnston 2007). In these models each component of the pulse profile originates from a different physical location in the magnetosphere. Because the components overlap in many cases and because their shapes are not uniquely defined, it is difficult to objectively classify profiles. Following Karastergiou & Johnston (2007), we have classified the profiles by eye into three classes depending on the number of distinct (possibly overlapping) peaks in the pulse profile. These classes are named “single”, “double” and “multiple”, depending on if one, two or more peaks were identified. Although this classification is subjective, it should be considered as a rough measure for the complexity.

Table 2 shows the percentage of pulsars in each class for three different \dot{E} bins. For the pulsars which are significantly scattered at 20 cm we used 10 cm data (when available) and we omitted profiles with $S/N < 30$ to improve significance. Compared with Karastergiou & Johnston (2007) we find relatively more singles and less multiples and also the difference between high and low \dot{E} pulsars is less pronounced. This might partially reflect the subjectivity of profile classification, but it may also be related to the fact that the classification of Karastergiou & Johnston (2007) was based on polarization properties. For instance, rapid changes in the PA-swing are often found in between components and can therefore be interpreted as an indication for the presence of multiple components. The polarization properties are discussed in a separate section in this paper.

4.1.2 Mathematical decomposition of the profiles

Because profile components can overlap and can have various shapes, it is in many cases not clear how many separate emission components there are. Also, because the classification is done by eye it is highly subjective at which level of detail the profile is separated into components. A more objective way to decompose the profile into components is to describe the profiles as linear combinations of basis functions. The number of required functions to fit the profile is then a measure for the complexity of the pulse profiles.

Gaussian functions are often used to decompose profiles

(e.g. Kramer et al. 1994), but we have chosen to use von Mises functions (von Mises 1918), which are defined as

$$I(x) = I_{\text{peak}} e^{\kappa \cos(x-\mu) - \kappa}. \quad (3)$$

Here μ is the location of the peak (in radians), I_{peak} is the peak intensity and κ is the concentration (which determines the width of the peak). The shape of these functions is very similar to Gaussians (see Fig. 2), but they can often fit the edges of components slightly better. The main difference is that von Mises functions are circular, hence they are also known as circular normal distributions. A fitting routine for von Mises functions is part of the *PSRCHIVE* software package.

There is a subtle difference between the required number of fit functions and the number of components in the pulse profile. The first is just a mathematical measure of complexity, while the latter is the number of distinct physical emission locations in the pulsar magnetosphere which are visible in the line of sight. These numbers can be different, because there is no a priori reason to believe that the shape of a profile component can be described by a single, simple, mathematical basis function which is the same for all pulsars. For instance, a profile which shows a tail because of interstellar scattering can have one component (“single profile”), but it can only be fitted by a number of von Mises functions. Another example can be seen in the decomposition as shown in Fig. 2. Although the component between pulse longitude 70° and 120° is fit by two von Mises functions, the smooth shape does suggest that it is a single asymmetric emission component. By using more complex asymmetric mathematical functions it might be possible to decompose some profiles in a smaller number of fit functions. However, in effect this is the same as to fit a larger number overlapping more simple symmetric functions which have less fit-parameters per function.

There is not always one unique solution for the decomposition of a profile and therefore the decomposition does not necessarily give additional insight in how profiles are composed out of distinct physical components. Nevertheless a noise free mathematical description of a pulse profiles can be used as a measure for its complexity. Moreover it is a very useful technique which makes it easier to measure profile properties such as pulse widths. An additional advantage of a mathematical description of the profile is that one can more accurately determine the component widths for pulsars which have overlapping components.

When using the number of mathematical fit functions as a measure of complexity it is important to take into account the S/N ratio of the profiles. A higher S/N profile will require a larger number of mathematical basis functions to fit its shape, even though the profile is not necessarily more complex. In order to avoid this effect, we determined how many of the fit functions would have a significant contribution to the total integrated intensity of the pulse profile when the S/N would have been 30. We only considered profiles with a $S/N \geq 100$ to ensure that all weak components which are just significant when the S/N would have been 30 are spotted by eye.

Fig. 3 shows the average number of von Mises functions required to fit the profiles when the S/N is scaled down to 30 for different \dot{E} bins. There is not much evidence that the profile complexity is very different for high and

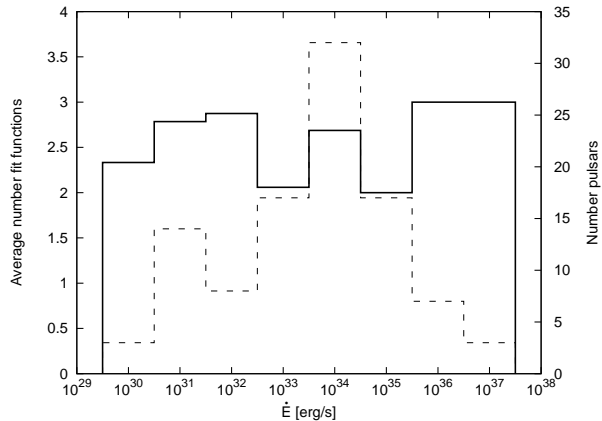


Figure 3. The histogram of the average number of von Mises functions required to fit the profiles when the S/N is scaled down to 30 for different \dot{E} bins (solid line). The dashed histogram shows the number of pulsars contributing in each bin. Only profiles with a $S/N \geq 100$ are included.

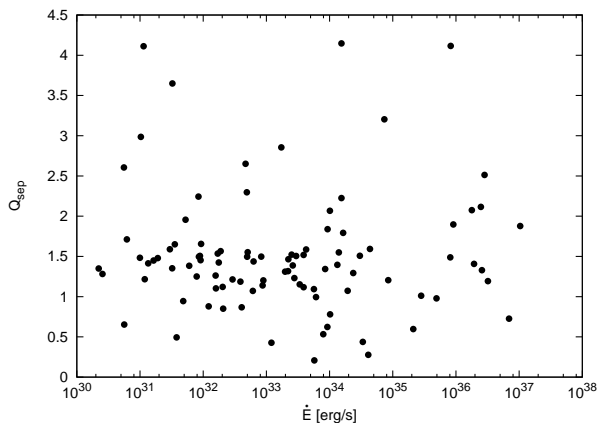


Figure 4. The dimensionless double separation (the ratio of the separation between the components and the average of their full width half maxima) versus the spin-down energy loss rate for all the observed pulsars at 20 cm which are classified to be doubles with a $S/N \geq 30$.

low \dot{E} pulsars. The absence of a significant correlation between \dot{E} and the number of fit functions is confirmed by calculating the Spearman rank-order correlation coefficient (Press et al. 1992) of the unbinned data, which is a non-parametric measure of correlation. Among the most complex profiles, according to this classification scheme, are those of PSRs J1034–3224 and J1745–3040, which indeed have complex looking profile shapes. An other pulsar which is ranked at the same level of complexity is PSR J1302–6350, which has to the eye a relatively simple double peaked profile, but its highly asymmetric components require relatively many mathematical functions to fit. We will therefore try a different method to define profile complexity below.

4.1.3 The dimensionless double separation

As described in section 4.1.2, the profiles of the high \dot{E} pulsars J1015–5719 and J1302–6350 were ranked as highly complex, while they appear to be “simple” to the eye. One prop-

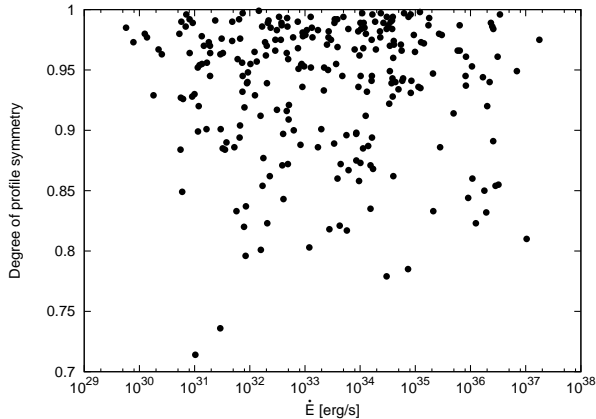


Figure 5. The degree of profile symmetry versus \dot{E} . Pulsars with a $S/N < 30$ and profiles with substantial scattering were excluded and only 20 cm data was considered. There is no evidence that high \dot{E} pulsars are more symmetric.

erty of these profiles which makes them look simple is that they are doubles with well separated components. We therefore tested the hypothesis that the doubles of high \dot{E} pulsars have more clearly separated components than those of the low \dot{E} pulsars. How clearly the components of doubles are separated can be quantified by calculating a quality factor, which we define to be

$$Q_{\text{sep}} = \frac{\Delta\phi_{\text{sep}}}{\frac{1}{2}(\text{FWHM}_1 + \text{FWHM}_2)}. \quad (4)$$

This dimensionless double separation is the ratio of the separation between the components $\Delta\phi_{\text{sep}}$ and the average of the full width half maxima of the components FWHM_1 and FWHM_2 . Higher values of Q_{sep} imply that the components are separated more compared with the width of the components.

Fig. 4 shows Q_{sep} versus \dot{E} for all profiles at 20 cm which were classified to be doubles and have a $S/N \geq 30$. There is no evidence that the components of doubles of low \dot{E} pulsars are more likely to be overlapping, which is confirmed by calculating the Spearman rank-order correlation coefficient. According to this measure the most clearly separated doubles are PSRs J1302–6350, J1733–3716, J1901–0906 and J2346–0609.

4.1.4 Profile symmetry

A factor which was not taken into account in the previous sections is the amount of symmetry in the profile. For instance, PSR J1302–6350 has highly asymmetric profile components, but the profile as a whole appears symmetric and could therefore be regarded as “simple”. It is therefore interesting to consider the degree of symmetry of the profiles, which can be measured by cross-correlating the profile with its mirror-image. We define the degree of profile symmetry to be the ratio of the maximum value of the cross-correlation function between the profile and the time reversed profile, and the maximum value of auto-correlation function of the profile. The degree of symmetry is therefore normalized to 1 for completely symmetric profiles and it decreases for more asymmetric profiles.

The degree of symmetry versus \dot{E} is shown in Fig. 5. The

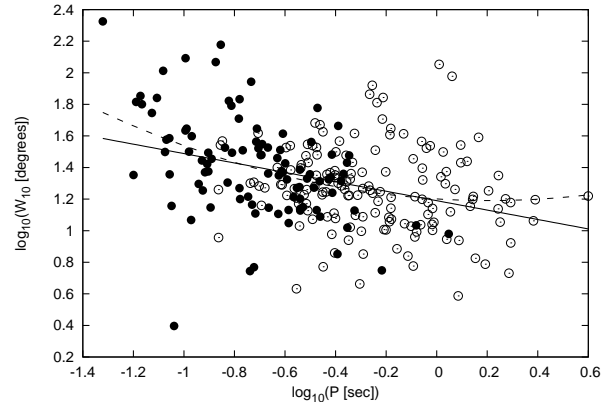


Figure 6. The measured profile 10% widths versus P . The solid line is the power law fit through the data, which has a slope of -0.30 . The dashed line indicates the fit of a second order polynomial through the data points (which is statistically not better than the power law fit). The filled points are pulsars with an $\dot{E} \geq 10^{34}$ erg s $^{-1}$ and the open points have a lower \dot{E} . Pulsars with a $S/N < 30$ and profiles with substantial scattering were excluded. All the shown observations were done at a wavelength of 20 cm.

pulsar with the lowest measured degree of symmetry is PSR B1747–31, which has a relatively narrow and bright leading component and a much broader and weaker trailing component. Also the complex main pulse of PSR B1055–52 can be found at the lower end of this figure. There is no indication for any correlation, which is confirmed by the Spearman rank-order correlation coefficient. Like for the other measures of complexity, it is hard to quantify that pulse profiles of high \dot{E} pulsars are more simple than those of the low \dot{E} pulsars.

4.2 Pulse widths versus P

A basic property of the emission beam of a pulsar is its half opening angle ρ . It is found that the opening angle is proportional to $P^{-1/2}$ (e.g. Biggs 1990; Kramer et al. 1998; Gil et al. 1993; Rankin 1993a), which is expected if the edge of the active area of the polar cap is set by the last open field lines. In order to derive the opening angle from the measured profile width one needs to know how the emission beam intersects the line of sight. Because the orientation of the line of sight with respect to the pulsar beam is for most pulsars at best only poorly constrained, it is difficult to obtain accurate opening angles. For a large sample of pulsars the unknown geometrical factors should average out and therefore the profile width and ρ should have the same P dependence. The unknown geometry will cause additional scattering around the correlation between the pulse width and P .

The measured pulse widths at 10% of the peak intensity (W_{10}) indeed show a slight anti-correlation with P (Fig. 6), while there is no indication for a dependence with \dot{P} (not shown). The slope is measured by reduced χ^2 fitting (the data points are weighted equally), which results in a slope of -0.30 ± 0.05^4 , comparable with the fit obtained from the

⁴ The correlation is slightly different, although within the error

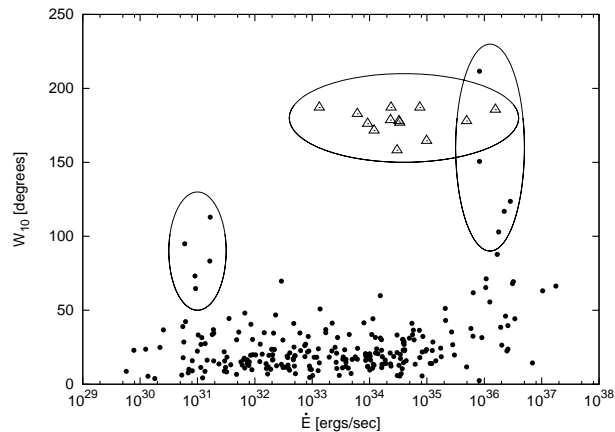


Figure 7. The measured profile 10% widths versus \dot{E} . The triangles indicate the pulsars which are classified to have interpsuls. Pulsars with a $S/N < 30$ and profiles with substantial scattering were excluded. All the shown observations were done at a wavelength of 20 cm. Three clusterings of pulsars are highlighted by ellipses, which are discussed in the text.

data of Gould & Lyne (1998) by Weltevrede & Johnston (2008). The slope of the correlation is therefore slightly less than what is expected from theory. This conclusion, in combination with the period distribution of pulsars with interpsuls, provides convincing evidence in favour for the evolution of the pulsar beam towards alignment with the rotation axis (Weltevrede & Johnston 2008).

If there is any deviation from a power law relationship between W_{10} and P , then it would be that the slope of the correlation is steeper for faster rotating pulsars. Although the fit of a second order polynomial through the data-points indeed show this trend, it is statistically not much better than the first order fit. High \dot{E} pulsars are in general spinning faster than low \dot{E} pulsars, and therefore one could conclude that the pulse widths of high \dot{E} pulsars have a stronger dependence on P than the low \dot{E} pulsars. To illustrate this the pulsars with high and low values of \dot{E} are marked differently in Fig. 6. One could argue that there is not much evidence for a correlation for the low \dot{E} pulsars, while this is clearer for the high \dot{E} pulsars. But, as the fit second order polynomial was statistically not much better than the fit of a power law, this conclusion is also not significant. If this correlation exist, then it would suggest that the profile widths of the high \dot{E} pulsars follow the theoretical prediction more closely than those of the low \dot{E} pulsars, which could indicate that the emission geometry for high \dot{E} pulsars is more simple.

4.3 Pulse widths versus \dot{E}

In the previous subsection we found that W_{10} is correlated with P . One can expect that the correlation with \dot{E} is weaker, because W_{10} was found to be uncorrelated with \dot{P} . Indeed, Fig. 7 shows that for most pulsars W_{10} is as good as uncorrelated with \dot{E} . But remarkably, unlike in Fig. 6 there

identical to the value quoted in Weltevrede & Johnston (2008). This is because since the publication of that paper more timing observations have been added.

are a number of outliers which are clustered in relatively well defined regions in \dot{E} -space. These outliers are indicated by the ellipses and each group will be discussed separately below.

The first group of outliers are the pulsars in the ellipse at the left hand side of Fig. 7. Although the profiles are clearly wider than most pulse profiles, they form a continuous distribution with the narrower profiles. These low \dot{E} pulsars are PSRs J1034–3224, J1655–3048 and J2006–0807 (which have complex looking profiles) and PSRs J1133–6250 and J1137–6700 (which are doubles with a clear saddle between the components). The profiles of these pulsars are most likely broad because their beam is close to alignment with the rotation axis, making the beam intersect the line of sight for a relatively long fraction of the rotation period. There is evidence that the beam evolves to alignment with the rotation axis over time (e.g. Weltevrede & Johnston 2008), so it is not surprising that these aligned pulsars are old pulsars with low \dot{E} values. For two of these pulsars estimates for the angle between the magnetic axis and the rotation axis can be found in the literature. These polarization studies indeed suggest that the beam of PSRs J1034–3224 (Manchester et al. 1998) and J2006–0807 (Rankin 1993b; Lyne & Manchester 1988) are close to alignment.

The second group of pulsars with wide profiles are the pulsars with interpsuls, which are marked with triangles in Fig. 7. These are PSRs J0834–4159, J0905–5127, B0906–49, B1124–60, J1549–4848, B1607–52, B1634–45, B1702–19, B1719–37, B1736–29, J1828–1101 and J1843–0702. The profiles of these pulsars are characterised by having an interpulse which is separated by approximately 180° in pulse longitude from the main pulse. This separation is much larger than the widths of the main- and interpulse. The most natural explanation for these interpsuls is that the emission of the main- and interpulse originates from opposite magnetic poles. These pulsars are concentrated to high values for \dot{E} . This is partially a selection effect in the sample of pulsars which are included in the Fermi timing program, but it has also shown by Weltevrede & Johnston (2008) that interpsuls are more likely to be detected in young (high \dot{E}) pulsars.

The third group of pulsars with wide profiles can also be found at the high \dot{E} end of Fig. 7. These are PSRs J1015–5719, B1259–63, J1803–2137, J1809–1917 and J1826–1334. Like the group of pulsars with wide profiles at the low \dot{E} end of the figure, this group appears to form a continuum with the pulsars with narrow profiles. We will refer to this group as the *energetic wide beam pulsars*. Their profiles show a double structure and they are exceptionally wide, but they are not separated by exactly 180° in pulse longitude. In contrast to the group of interpsuls, this separation is not much larger than the width of the individual components. The two components are often highly asymmetric with steep edges at opposite sides, making the profile as a whole to have a high degree of mirror symmetry. For some of these pulsars a weak bump is detected in between the components, which disappears at higher frequencies. The dependence of the PA on pulse longitude is usually simple and straight.

It is not clear if PSR B1055–52 should be classified as an energetic wide beam pulsar or a pulsar with an interpulse. On the one hand the separation between the main- and interpulse is larger than the width of the individual components,

but on the other hand the components are very wide and the interpulse is not exactly 180° away from the main pulse. The location of PSR B1055–52 in Fig. 7 (the lowest triangle at $\dot{E} = 3.0 \times 10^{34} \text{ erg s}^{-1}$) suggest that it is well separated from the other energetic wide beam pulsars, although the group of interpulse pulsars appear to have an overlap with the group of energetic wide beam pulsars. Especially the location of PSRs B0906–49 ($\dot{E} = 4.9 \times 10^{35} \text{ erg s}^{-1}$) and J1828–1101 ($\dot{E} = 1.6 \times 10^{36} \text{ erg s}^{-1}$) in the figure are consistent with both groups. Both these pulsars have interpulses at $\sim 180^\circ$ away from the main pulse and this separation is much larger than the component widths (the broad components of J1828–1101 at 20 cm are because of scatter broadening), which is good evidence that both interpulses are emitted from the opposite pole. For PSR B0906–49 the PA-swing is shown to be inconsistent with a wide cone interpretation (Kramer & Johnston 2008).

The energetic wide beam pulsars are among the pulsars with the highest \dot{E} values ($\dot{E} > 5 \times 10^{35} \text{ erg s}^{-1}$), although it is not true that all pulsars with high \dot{E} values are also energetic wide beam pulsars. This is first of all shown by the overlap between the group of pulsars with interpulses and the energetic wide beam pulsars group. Secondly, PSR J1513–5908 which has the highest \dot{E} value in our sample, does not show any evidence of a double structure. Finally, PSR J1028–5819 is an extremely narrow double (Keith et al. 2008, point in the bottom left corner of Fig. 6). A high \dot{E} therefore appears to be an important parameter which allows an energetic pulsar to form a wide beam, but there must be more factors involved.

4.4 The intensity ratio of the components of high \dot{E} pulsars with double profiles

Johnston & Weisberg (2006) noted that the trailing component of well separated double profiles of high \dot{E} pulsars tend to dominate in total power (and in circular polarization as we will discuss below). This curious effect seems to be strongest for pulsars with $\dot{E} > 10^{35} \text{ erg s}^{-1}$ (see for example PSR J1420–6048, Fig. A6). The only exceptions are the Vela pulsar (which has no well separated double profile), PSR J1302–6350 (an energetic wide beam pulsars for which it is not clear which component is the trailing component) and PSR J1831–0952. Nevertheless, in the majority of the cases this correlation holds.

5 POLARIZATION

5.1 Linear polarization

It has been pointed out by several authors that degree of linear polarization is high for high \dot{E} pulsars (e.g. Qiao et al. 1995; von Hoensbroech et al. 1998; Crawford et al. 2001; Johnston & Weisberg 2006). This correlation is clearly confirmed, as can be seen in Fig. 8. There is a transition from a low to a high degree of linear polarization which happens around $\dot{E} \sim 10^{34} - 10^{35} \text{ erg s}^{-1}$. Virtually all pulsars with $\dot{E} < 5 \times 10^{33} \text{ erg s}^{-1}$ have less than 50% linear polarization and for almost all pulsars with $\dot{E} > 2 \times 10^{35} \text{ erg s}^{-1}$ this percentage is above 50%. There appears to be a transition region in between where pulsars can both have low

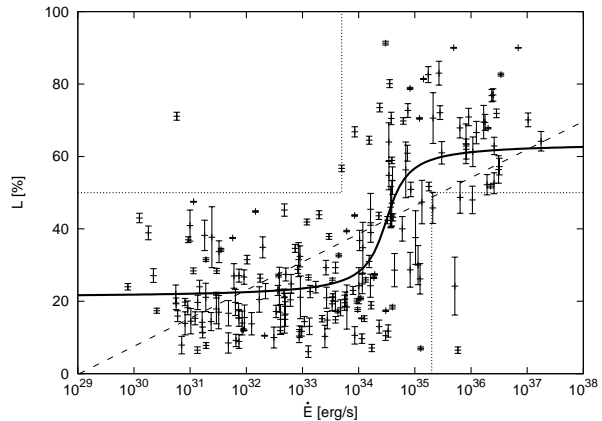


Figure 8. The degree of linear polarization versus \dot{E} of all pulsars observed at 20 cm for which a significant degree of linear polarization was measured. Pulsars which show evidence for scatter broadening were excluded. There are two relatively well defined regions which are almost empty in this diagram. The dashed line shows the linear fit and the solid curve the fit of an arctan function illustrating the step in the degree of linear polarization.

and high degrees of polarization, although the transition is remarkably sharp and there are well defined spaces in the figure which are almost empty. The non-linearity of the degree of linear polarization versus \dot{E} is confirmed by fitting an arctan function through the data (solid curve in Fig. 8). This is done by minimizing the χ^2 using the Levenberg-Marquardt algorithm (Marquardt 1963) as implemented in Press et al. (1992) (the data points are weighted equally). The total χ^2 is reduced by 20% compared with a linear fit, which shows that the step in the degree of linear polarization is important to consider. Adding higher order polynomial terms does not reduce the χ^2 further, suggesting that the step is the most dominant deviation from non-linearity. The position of the steepest point in the fitted function occurs at $\log_{10} \dot{E} = 34.50 \pm 0.08$.

The emission of pulsars is thought to be a combination of two orthogonally polarized modes (OPM, e.g. Manchester et al. 1975). This aspect of the emission can manifest itself in sharp $\sim 90^\circ$ jumps in the position angle (PA) over a small pulse longitude range. These jumps are thought to be sudden transitions from the domination of one mode to the other. Jumps in the PA-swing therefore indicates that both modes are present in the emission. The mixing of both modes at a certain longitude will lead to depolarization, so the presence of jumps in the PA-swing could be anti-correlated with the degree of polarization. By comparing the top and bottom panel of Fig. 9 one can see that the \dot{E} value at which the transition from a low to a high degree of polarization takes place coincides with the \dot{E} value after which pulsars do not have jumps in their PA. This is therefore important evidence that the increase in the degree of linear polarization with \dot{E} is caused by one OPM dominating the emission. Most high \dot{E} pulsars do not show OPM jumps, but the reverse is not always true. Low \dot{E} pulsars can have a low degree of linear polarization without evidence for OPM jumps.

There are three curious exceptions in Fig. 8 which do not follow the general trend. First of all PSRs J1509–5850 and J1833–0827 have a low degree of linear polarization while they have a high \dot{E} (5.2×10^{35} and $5.8 \times 10^{35} \text{ erg s}^{-1}$

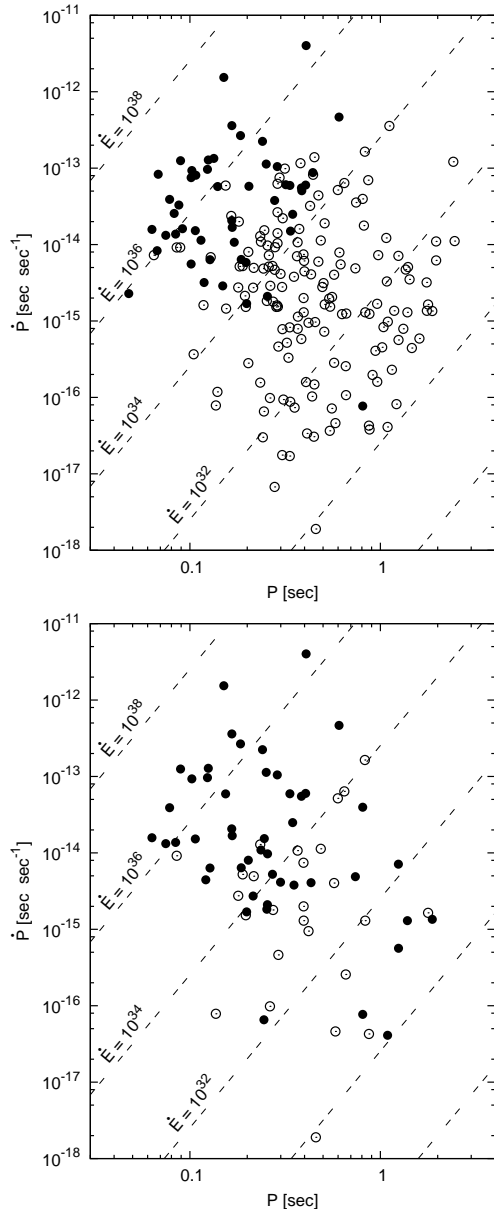


Figure 9. *Top:* The $P - \dot{P}$ diagram of all the observed pulsars at 20 cm for which a significant degree of linear polarization could be measured. The filled and open circles are the pulsars which are respectively more or less than 50% linearly polarized. *Bottom:* The $P - \dot{P}$ diagram of the pulsars which show sudden jumps in their PA-swing (open circles) and those which have a smooth PA-swing (filled circles).

respectively). However it must be noted that the leading and trailing components of PSR J1833–0827 are highly polarized at 10 cm. The degree of linear polarization of this pulsar shows a drop to zero in the middle of central component, which could indicate that there is a transition in the dominating OPM. The other exception is PSR J0108–1431, which has a low \dot{E} but is nevertheless highly polarized. This could suggest that this pulsar has some similarities with high energy pulsars.

All pulsars without a significant amount of measured degree of linear polarization fall below the $\dot{E} < 5 \times 10^{33}$ erg s^{-1} line. The only exception is PSR J1055–6032, which ap-

pears to have a very low degree of polarization. The rule that high \dot{E} pulsars are highly polarized therefore is confirmed in the majority of all pulsars.

5.2 Emission heights

5.2.1 The emission height derived from the pulse width

The wider pulse profiles of high \dot{E} pulsars are often attributed to a larger emission height for those pulsars (e.g. Manchester 1996; Karastergiou & Johnston 2007). The divergence of the magnetic (dipole) field lines away from the magnetic axis makes the half opening angle ρ of the beam scale with the square root of the emission height. Under the assumption that the beam of the pulsar is confined by the last open field lines it follows that

$$\rho = \sqrt{\frac{9\pi h_{em}}{2 P c}} \quad (5)$$

(e.g. Lorimer & Kramer 2005), where h_{em} is the emission height and c the speed of light.

Wider beams are more likely to produce wide profiles, although the observed pulse width also depend on the orientation of the magnetic axis and the line of sight with respect to the rotation axis. The relevant parameters are the angle α between the magnetic axis and the rotation axis and the angle ζ between the line of sight and the rotation axis. A related angle is the impact parameter $\beta = \zeta - \alpha$, which is the angle between the line of sight and the magnetic axis at its closest approach. For most pulsars it is extremely difficult to obtain reliable values for these angles, which makes it hard to derive the emission height from W_{10} .

For a sample of pulsars with a random orientation of the magnetic axis and the line of sight both the α and ζ distribution are sinusoidal. Simulations using the model described in Weltevrede & Johnston (2008), show that the pulse width distribution for such a sample pulsars peaks at 2ρ . Some pulsars will have wider profiles because the pulsar beam is more aligned with the rotation axis, while others will have narrower profiles because the line of sight grazes the beam. This implies that the typical pulse width of a large sample of pulsars which have random orientations of their spin and magnetic axis and have similar opening angles ρ should be equal to 2ρ . In other words, a typical profile width is equal to that which is expected for an orthogonal rotator ($\alpha = 90^\circ$) and a line of sight which makes a central cut through the emission beam ($\beta = 0^\circ$). For such geometry Eq. 5 can be rewritten to

$$h_{90} = \frac{cP(W_{10})^2}{18\pi}, \quad (6)$$

which is the emission height for a typical random geometry assuming a magnetic dipole field and an active area of the polar cap which is set by the last open field lines.

5.2.2 The emission height derived from the PA-swing

An independent way to estimate the emission height is by measuring the shift of the PA-swing caused by the co-rotation of the emission region with the neutron star. In this method it is assumed that the PA-swing is described by the rotating vector model (RVM; Radhakrishnan & Cooke

Name	\dot{E} [erg s $^{-1}$]	h_{PA} [km]	h_{90} [km]	$\Delta\phi$ [deg]	R_{LC} [km]
J1015–5719	8.27×10^{35}	–	5160	–	6674
J1302–6350	8.25×10^{35}	–	3476	–	2279
J1803–2137	2.22×10^{36}	461	2967	8.3	6375
J1809–1917	1.78×10^{36}	130	1425	3.8	3948
J1826–1334	2.84×10^{36}	191	2522	4.5	4841
J0304+1932	1.91×10^{31}	75	562	0.1	66206
J0536–7543	1.15×10^{31}	-21	1472	-0.0	59444
J0614+2229	6.24×10^{34}	1051	99	7.5	15982
J0630–2834	1.46×10^{32}	118	2459	0.2	59376
J0631+1036	1.73×10^{35}	1087	278	9.1	13731
J0729–1448	2.81×10^{35}	1143	291	10.9	12008
J0742–2822	1.43×10^{35}	338	68	4.9	7957
J0835–4510	6.91×10^{36}	32	30	0.9	4263
J0908–4913	4.92×10^{35}	320	24	7.2	5094
J1048–5832	2.01×10^{36}	-24	141	-0.5	5901
J1105–6107	2.48×10^{36}	243	52	9.2	3015
J1119–6127	2.34×10^{36}	2082	1406	12.3	19455
J1123–4844	1.76×10^{32}	540	152	5.3	11682
J1253–5820	4.97×10^{33}	690	116	6.5	12191
J1320–5359	1.67×10^{34}	673	158	5.8	13347
J1359–6038	1.21×10^{35}	544	41	10.2	6084
J1420–6048	1.04×10^{37}	106	442	3.7	3253
J1531–5610	9.09×10^{35}	81	136	2.3	4018
J1535–4114	1.98×10^{33}	474	235	2.6	20654
J1637–4553	7.51×10^{34}	392	62	7.9	5667
J1701–3726	2.97×10^{31}	184	984	0.2	117118
J1705–3950	7.37×10^{34}	-120	690	-0.9	15218
J1709–4429	3.41×10^{36}	563	326	13.2	4889
J1733–3716	1.54×10^{34}	932	1969	6.6	16107
J1740–3015	8.24×10^{34}	818	31	3.2	28952
J1835–1106	1.78×10^{35}	445	93	6.4	7916
J1841–0345	2.69×10^{35}	353	415	4.2	9737

Table 3. The emission height h_{PA} is derived from the offset $\Delta\phi$ between the inflection point of the PA-swing and the centre of the pulse profile. The emission height h_{90} is derived from the pulse width assuming an orthogonal rotator ($\alpha = 90^\circ$) and a line of sight which makes a central cut through the emission beam ($\beta = 0^\circ$), which is the emission height for a typical random geometry. The last column is the light cylinder radius. The first five pulsars are the pulsars which we have classified as energetic wide beam pulsars.

1969). The position angle ψ is then predicted to depend on the pulse longitude ϕ as

$$\tan(\psi - \psi_0) = \frac{\sin \alpha \sin(\phi - \phi_0)}{\sin \zeta \cos \alpha - \cos \zeta \sin \alpha \cos(\phi - \phi_0)}, \quad (7)$$

where ψ_0 and ϕ_0 are the PA and the pulse longitude corresponding to the intersection of the line of sight with the fiducial plane (the plane containing the rotation and magnetic axis). The PA-swing is a S-shaped curve and its inflection point occurs at ϕ_0 . The RVM fit is shown in the figures of Appendix A and B for the pulsars which have a roughly S-shaped PA-swing.

If the emission profile is symmetric around the magnetic axis, then one could expect the inflection point to coincide with the middle of the pulse profile. However, co-rotation causes the inflection point to be delayed with respect to the pulse profile. The pulse longitude difference $\Delta\phi$ between the middle of the profile and the inflection point of the PA-swing

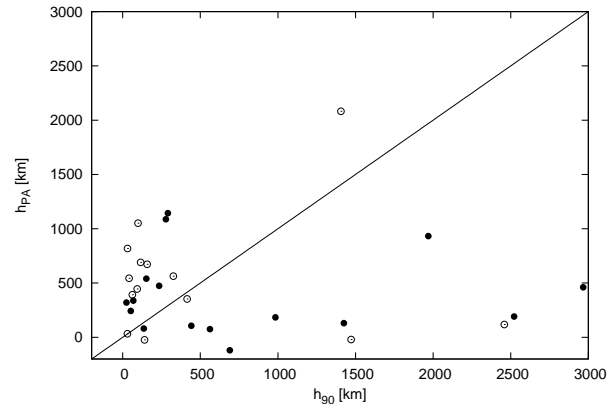


Figure 10. The emission height as derived using two independent methods, one using the pulse widths (h_{90}) and the other using the shift of the PA-swing with respect to the profile (h_{PA}). The solid circles indicate profiles with a clear double structure. The points should lie on the line if the emission heights are consistent with each other.

can be used to derive the emission height (Blaskiewicz et al. 1991)

$$h_{\text{PA}} = \frac{P c \Delta\phi}{8\pi}. \quad (8)$$

The relative shift of the PA-swing with respect to the profile is independent of α and ζ (Dyks et al. 2004). If the emission height is too large it could be difficult to measure $\Delta\phi$ because the inflection point of the PA-swing is shifted beyond the edge of the pulse profile.

5.2.3 The derived emission heights

The emission height derived using the PA-swing (h_{PA}) and using the pulse width (h_{90}) are both listed in Table 3. This only includes the pulsars which have a clear S-shaped PA-swing at 20 cm. The typical emission height is a few hundred km, which is similar to the emission height found by other authors (e.g. Blaskiewicz et al. 1991; Mitra & Rankin 2002). One can see that for some pulsars h_{PA} is negative, which is obviously impossible. This can be considered to be a clear warning that the emission heights for an individual source could be completely wrong, but one can nevertheless hope that they are meaningful in a statistical sense. In order to test this we calculated the Spearman rank-order correlation coefficient between h_{PA} and h_{90} , which shows that there is no evidence for any correlation between these parameters. This is also evident from Fig. 10, where these quantities are plotted against each other. We are therefore forced to accept that even in a statistical sense the calculated emission heights are inconsistent, supporting the same conclusion reached by Mitra & Li (2004) based on six pulsars.

There are a number of reasons why the heights derived using the two methods could be inconsistent. If the beams are significant patchy, then the centroid of the profile is not related to the position of magnetic axis and both methods to derive emission heights will fail. We therefore made a distinction in Fig. 10 between the profiles which are clear doubles and other profiles, because the double structure could indicate that the pulsar beam is roughly symmetric around

the magnetic axis. As one can see there is no noticeable difference in the distributions. Another effect that could be important is the effect of sweepback of the magnetic field lines. Dyks & Harding (2004) derived that the effect of sweepback can dominate over other effects of co-rotation at low altitudes, making it possible for the inflection point of the PA-curve to precede the profile centre. The PA-curve can also precede the profile in case of inward directed emission (Dyks et al. 2005).

Despite the inconsistency between the derived emission heights using both methods, it is not true that the emission heights are entirely random. Most pulsars show a positive emission height h_{PA} , indicating that the steepest slope of the PA-swing trails the centroid of the profile in most cases. In fact, Fig. 10 appears to show evidence that it is unlikely that both h_{90} and h_{PA} are large. In Table 3 one can see that the emission of the energetic wide beam pulsars should come from near the light cylinder in order to explain the width of the pulse profiles ($h_{90} \sim R_{LC}$). However, the derived emission heights from the the PA-swing fits are not unusually large. In this list one could add the emission height of PSR J1015–5719, which is estimated by Johnston & Weisberg (2006) to be 380 km.

All the energetic wide beam pulsars with a derived emission height from the PA-swing can be found below the solid line in Fig. 10, as well as PSRs J1705–3950 and J1733–3716 which have similar profile shapes. It seems unlikely that they all have beams which are close to alignment with the rotation axis, which suggest a different reason for the large widths of the profiles of the energetic wide beam pulsars. Apparently the emission heights which are derived from the PA-swings of the energetic wide beam pulsars are systematically underestimated, or the heights derived from the profile widths are over estimated. The first case could be explained by magnetic field line sweepback when the emission height is low (Dyks & Harding 2004). The second case implies that the beams of these pulsars are wider than could be expected from the divergence of the dipole field lines. The widening of the pulsar beam could, at least in principle, be caused by propagation effects in the magnetosphere.

Another explanation for the deviation of the energetic wide beam pulsars from the line in Fig. 10 could be that the two methods estimate the emission heights at different locations in the magnetosphere. The method based on the profile width estimates the emission height at the edge of the of the beam, while the method using the PA-swing estimates the emission height of the more central regions of the beam. For the energetic wide beam pulsars h_{90} was found to be systematically larger than h_{PA} , which can be interpreted as evidence for an increase in the emission height at the edge of the beam. This interpretation will be discussed in more detail in the following section.

Fig. 10 shows that besides the group of pulsars which have relatively large h_{90} compared to h_{PA} , there is also a group in where the opposite is seen. An explanation could be that for those pulsars only a fraction of the polar cap is active (e.g. Kijak & Gil 1997). Support for this interpretation is that the profiles of a number of pulsars in this group are argued to be produced by partial cones, including PSR J0543+2329 (Weisberg et al. 2004), J0614+2229 (Johnston et al. 2007) and J0659+1414 (Everett & Weisberg 2001).

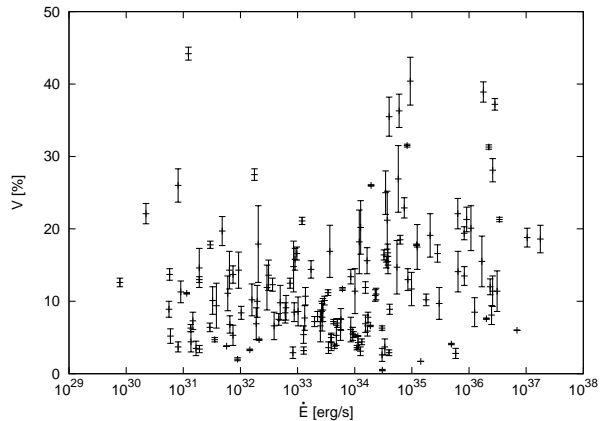


Figure 11. The degree of circular polarization (the absolute value of Stokes V) versus \dot{E} of all pulsars observed at 20 cm for which a significant degree of circular polarization was measured. Pulsars which show evidence for scatter broadening were excluded.

5.3 Circular polarization

Unlike the degree of linear polarization the degree of circular polarization appears to be unaffected by \dot{E} . Also the fraction of pulsar which are left- and right-hand circularly polarized is about 50 per-cent for both the high and low \dot{E} pulsars.

Johnston & Weisberg (2006) noted that, besides the total intensity, also the degree of circular polarization usually dominates in the trailing components of high \dot{E} pulsars with well separated double profiles. This correlation is also clearly confirmed in our data for all pulsars with an $\dot{E} > 10^{34}$ erg s $^{-1}$. The only clear counter example in our data-set could be PSR J1705–1906 ($\dot{E} = 7 \times 10^{34}$ erg s $^{-1}$), which has a high degree of circular polarization in the leading half of the profile. However, it must be noted that the single pulse modulation properties of this pulsar suggest that the leading component is not the leading component of a double, but rather a precursor to a blended double which forms the trailing half of the profile (Weltevrede et al. 2007).

Remarkable correlations have been reported between the sign of the circular polarization and the sign of the slope of the PA-swing. According to Radhakrishnan & Rankin (1990) the sign of the slope of the PA-swing is correlated with the sign of the circular polarization for pulsars which are cone dominated and for which the sign of the circular polarization is the opposite in the two components. But Han et al. (1998) did not confirm this correlation. Instead they propose that there is a correlation between the sign of the circular polarization and the sign of the slope of the PA-swing for cone dominated pulsars which have the same sign of circular polarization. Our data does not show much evidence for either correlation. Compare for instance the plots for PSR J1826–1334 (positive circular polarization, decreasing PA-swing) with PSR J1733–3716 (negative circular polarization, decreasing PA-swing).

6 DISCUSSION

6.1 Extended radio emission regions?

We concluded that the differences in the pulse profile morphology of the high and low \dot{E} pulsars is in general rather

subtle, without an objectively measurable discriminator between them. An exception is what we call the group of energetic wide beam pulsars, which do have distinct profile properties and which will be discussed separately below. The measured slope of the $W_{10} - P$ correlation appears to be flatter than the theoretical $P^{-1/2}$ slope. It is far from straight-forward to link the deviation of the slope to a physical mechanism. For example, as explained in Weltevrede & Johnston (2008), the measured slope depends on the details of the evolution of the pulsar spin-down and the alignment of the magnetic axis with the rotation axis. If the active area of the polar cap is influenced by other factors than just the opening angle of the last open field lines, or if the emission height varies from pulsar to pulsar, one can expect to observe its effects in the $W_{10} - P$ correlation. There is some marginal evidence that the slope of the correlation is steeper for high \dot{E} pulsars, suggesting that for high \dot{E} pulsars these other factors are less important.

If one believes that the emission geometry is simpler for high \dot{E} pulsars, one can ask the question of what is causing this. One factor that could affect the complexity of profiles is the emission height. Complexity could arise because of multiple distinct emission heights within the beam (Karastergiou & Johnston 2007). In their model high \dot{E} pulsars have only one emission height which is similar for different pulsars. However, one could also make the argument for an opposite effect. Maybe the emission of high \dot{E} pulsars is not emitted from a well defined height, but rather from an extended height range. This would mean that the observed profiles of high \dot{E} pulsars are a superposition of profiles emitted from a continuum of heights. The observed sum of those profiles (shifted with respect to each other by aberration and retardation) will have less complexity because they are blurred out. Not only are the profiles expected to be less complex in this scenario, but there is also not much room to vary the emission height from pulsar to pulsar if the height range is large. This would make the $W_{10} - P$ correlation follow the prediction more closely. Large emission height ranges are typical for high energy models, such as the slot gap models (e.g. Muslimov & Harding 2004a) or the two pole caustic models (Dyks & Rudak 2003), hence there could be parallels with the radio emission for high \dot{E} pulsars. These parallels could be even more relevant for the energetic wide beam pulsars.

6.2 The energetic wide beam pulsars

As discussed by e.g. Manchester (1996), there is a group of young pulsars which can be found among the highest \dot{E} pulsars which have very wide profiles with often steep edges. The profiles are clearly mirror symmetric, suggesting that the components are the two sides of a single beam rather than two beams from opposing magnetic poles. This interpretation is also suggested by the frequency evolution of PSR B1259–63 (Manchester & Johnston 1995). Because these objects are young, the typical orientation of the magnetic axis is not expected to be very different for the highest \dot{E} pulsars and those with intermediate values, which suggests that some pulsars with high \dot{E} values can have very different beams compared with other pulsars.

An interesting analogue can be drawn between the radio profiles of energetic wide beam pulsars and the high

energy profiles of pulsars. High energy profiles can also be wide doubles which often have sharp edges (e.g. Thompson 2004). The pulsars which produce high energy emission are the pulsars with high \dot{E} values, so there could be a direct link between the high energy pulsars and the energetic wide beam pulsars. Maybe the radio emission and the high energy emission are produced at the same location in the magnetosphere. The sharp edges of the high energy profiles are often explained by caustics which form because of the combined effect of field line curvature, aberration and retardation (e.g. Morini 1983). These caustics occur when the emission is produced high in the magnetosphere over a large altitude range and if the magnetic axis is not aligned to the rotation axis (e.g. Dyks & Rudak 2003). If the radio emission and γ -ray emission would come from similar locations, one would expect the radio and γ -ray profiles to look alike. Hopefully the Fermi satellite will find high energy counterparts for these pulsars which allows a test of this hypothesis.

Another way to produce profiles with sharp edges could be the combination of refraction of radio waves in pulsar magnetospheres in combination with an emission height which is different for different field lines (Weltevrede et al. 2003). Only the ordinary wave mode is refracted (e.g. Barnard & Arons 1986) or scattered (Petrova 2008) in the magnetosphere. The profiles of the energetic wide beam pulsars can therefore be expected to be dominated by one polarization mode, which could potentially also explain their high degree of linear polarization. The unpolarized bump which is observed in the middle of some of these profiles could be the un-refracted part of the beam, which is depolarized because the presence of the extra-ordinary mode. These central components are strongest at lower frequencies, consistent with the steeper spectral index which is often observed for the central components of pulse profiles (e.g. Rankin 1983). However, it remains to be seen if propagation effects can be strong enough to explain the extreme pulse widths which are observed.

The emission geometry appears to be different for high \dot{E} pulsars and is possibly more similar to that of the high energy emission. However, not all pulsars with high \dot{E} values produce these extremely wide profiles. Apparently only a subset of the high \dot{E} pulsars have emission geometries which are very different from normal radio pulsars. A high \dot{E} is therefore an important parameter required for the energetic wide beam pulsars, but not the only one. For instance, maybe only certain configurations of the plasma distributions enlarge the beam via propagation effects or maybe not all pulsars have a slot gap which produces radio emission. It must also be noted that, like the high \dot{E} radio pulsars, not all the high energy pulse profiles of pulsars are doubles (e.g. PSR B1706–44).

6.3 Emission heights

There is no evidence that pulsars with large emission heights (derived from their PA-swing) have wider profiles. It is therefore not clear what the physical meaning of these emission heights is. There are many reasons why the derived emission heights could be wrong, including asymmetric beams, partially active polar caps or sweepback of the magnetic field lines. Also if the PA-swing of emission which is emitted far out in the magnetosphere the PA can be expected to deviate

from the rotating vector model. For instance, the PA-swing for the outer gap model is predicted to have the steepest slope near the edges of the profile (Romani & Yadigaroglu 1995), rather than at the pulse longitude corresponding to the location of the magnetic axis. This would complicate the calculation of emission heights from the observed PA-swing considerably. Nevertheless, the fact that most PA-swings trail the centroid of the profile suggest that the derived emission heights do carry some information.

The emission of the energetic wide beam pulsars should come from near the light cylinder in order to explain the width of the pulse profiles. However, the derived emission heights from the PA-swing fits seem to suggest that the emission heights are not unusually large. This can be seen as support that the beams of energetic wide beam pulsars are wide because of propagation effects instead of caused by a large emission height. An alternative interpretation is that the emission height at the edge of the beam is much larger than in the centre of the beam. This would fit in nicely with the result of Gupta & Gangadhara (2003), who concluded that the outer components of PSR B0329+54 are emitted from higher in the magnetosphere. It also fits in nicely with the hypothesis that the emission of the energetic wide beam pulsars comes from an extended emission height range, making the emission geometry very similar to the slot gap model.

6.4 Interpulse problem?

The conclusion that the beams of energetic wide beam pulsars are large appears to be unavoidable. If this is the case, than one would expect that it is very likely for the line of sight to intersect the beams of both poles of the pulsar. Using the model described by Weltevrede & Johnston (2008) the probability for the line of sight to intersect both beams is predicted to be 64%, assuming $\rho = 75^\circ$ and a random orientation of the magnetic axis and the line of sight. However, there is no clear example of an energetic wide beam pulsar which has a (double peaked) interpulse. The “interpulse problem” is then why we do not observe the interpulses of the energetic wide beam pulsars.

It is argued by Manchester (1996) that the steep edges form the outer edge of an extremely wide beam, which would make the peak-to-peak separation of the profiles wider than 180° . In that case the weak bumps observed for some of these pulsars are then separated by half a rotational phase from the centre of the profile, which would make them interpulses. However, because the bumps fill in the region in between the sharp edges, it seems more likely that the sharp edges form the inner edges of a wide beam. In that case the profiles are less wide and the bump forms the centre of the same wide beam.

The interpulse problem suggests that the beam sizes are different for the magnetic poles of the energetic wide beam pulsars. As discussed above, not all profiles of high \dot{E} pulsars have wide components. This implies that other criteria have to be met in order to make the beams wide. These criteria are not necessarily met simultaneously for both poles, which would reduce the fraction of pulsars with interpulses. The very different shape of the main- and interpulse of PSR B1055–52 show that interpulse beams can have very different shapes, hence possibly also very different sizes. Only 5 of the 26 pulsars with an $\dot{E} > 5 \times 10^{35}$ erg s⁻¹ in Fig. 7 are

classified to be energetic wide beam pulsars. Therefore the chance that both poles produces a wide beam is expected to be only $\sim 4\%$ if the chance of producing a wide beam is independent for each pole.

A more extreme point of view to solve the interpulse problem is put forward by Manchester (1996) who argues, following Manchester & Lyne (1977), that all pulsars only have one active wide beam. Although this would trivially solve the interpulse problem, it does not explain the concentration of main- interpulse separations near 180° (see Fig. 7).

6.5 Polarization

The degree of linear polarization is found in several studies to increase with \dot{E} . Such behaviour is predicted for the natural wave modes in the cold plasma approximation (von Hoensbroech et al. 1998). One of the most surprising results of this paper is the sudden increase in the degree of linear polarization with \dot{E} . This suggest that pulsars can be separated into two groups which have distinct physical properties. This could either be in the structure of the magnetosphere or the physics of the emission mechanism itself. It is remarkable that over 7 orders of magnitude in \dot{E} the degree in linear polarization is the only thing that is clearly changing.

It has been shown that the degree of polarization is clearly related to the presence of OPM transitions in the PA-swing. The two plasma modes (X-mode and O-mode) can be expected to be separated more in pulse longitude for high \dot{E} pulsars, because the difference in their refractive indices is larger (e.g. von Hoensbroech et al. 1998). This could prevent the modes from mixing, and therefore prevent depolarization. However, the fact that high \dot{E} pulsars are less likely to show jumps in their PA-swing suggests that they only effectively generate one of the modes. Johnston et al. (2005) found that the velocity vectors of most pulsars make an angle close to either 0° or 90° with the PA of the linear polarization (measured at the inflection point). This is interpreted as evidence for alignment of the rotation axis of the star with its proper motion vector and the bimodal nature of the distribution of angles is interpreted to be due to the domination of different plasma modes for different stars. This result therefore suggest that if the emission of high \dot{E} pulsars is dominated by one mode, it could be either of the two for different pulsars. If the profiles of the energetic wide beam pulsars are widened by refraction, than their emission should be dominated by the O-mode which can be refracted in the pulsar magnetosphere.

A very different interpretation of the sudden increase of the degree of linear polarization with \dot{E} is based on the fact that the \dot{E} at the transition is very similar to the death line for curvature radiation (Harding & Muslimov 2002). This death line could potentially cause a sudden change in for instance the plasma distribution in the magnetosphere (which is responsible for the refraction of the plasma waves), or it could possibly change the emission mechanism which is responsible for the radio emission. The possible link between the degree of linear polarization of the radio emission and the mechanism for the production of the high energy emission could therefore suggest that the γ -ray efficiency is correlated with the degree of linear polarization in the radio band.

It would therefore be extremely interesting to find out if a pulsar like PSR J0108–1431, which is highly polarized with a low \dot{E} , can be detected by the Fermi satellite.

6.6 Circular polarization

The trend noted by Johnston & Weisberg (2006) that the degree of circular polarization is usually higher in the second component of doubles is clearly present in our data as well. It is a possibility that this is a result of the co-rotation velocity of the emission region. As shown by for instance Dyks (2008), particles travelling along the magnetic field lines of a rotating dipole will follow stronger curved paths (in the inertial observer frame) at the leading half of the pulse profiles compared to the trailing half of the pulse profile. This is the reason why the observed PA-swing appears to be shifted with respect to the pulse profile (equation 8). The degree of circular polarization is in general highest in the central parts of the pulse profile, there where the curvature of the field lines is weakest. This could therefore suggest that the location of the highest degree of circular polarization is, like the PA-swing, shifted to later times by co-rotation.

7 CONCLUSIONS

In this paper we present and discuss the polarization profiles of a large sample of young, highly energetic pulsars which are regularly observed with the Parkes telescope. This sample is compared with a sample of a similar number of low \dot{E} objects in order to draw general conclusions about their differences.

There is some evidence that the total intensity profiles of high \dot{E} pulsars are slightly simpler based on a classification by eye. However, there is no difference in the complexity of the mathematical decomposition of the profiles, the amount of overlap between the components of doubles or the degree of profile symmetry. We therefore conclude that differences in the total intensity pulse morphology between high and low \dot{E} pulsars are in general rather subtle. High \dot{E} pulsars appear to show a stronger $W_{10} - P$ correlation which is closer to the theoretical expectation, suggesting that for high \dot{E} pulsars there are less complicating factors in the emission geometry.

A much more pronounced difference between high and low \dot{E} pulsars is the degree of polarization. The degree of polarization was already known to increase with \dot{E} , but our data shows there is a rapid transition between relatively unpolarized low \dot{E} pulsars and highly polarized high \dot{E} pulsars. The increase in the degree of polarization is related to the absence of OPM jumps. Refraction of the radio emission is expected to be more effective in the magnetosphere of high \dot{E} pulsars, which could prevent depolarization because of mixing of the plasma modes. The absence of OPM jumps suggest that one of the two modes (not necessarily the same for different pulsars) dominates over the other. The \dot{E} of the transition is very similar to the death line for curvature radiation, which could be the reason why the transition is relatively sharp. This potential link between the high energy radiation and the radio emission could mean that the γ -ray efficiency is correlated with the degree of linear polarization in the radio band.

The degree of circular polarization is in general higher

in the second component of doubles. This remarkable correlation is possibly caused by the effect of co-rotation on the curvature of the field lines in the inertial observer frame, making this effect very similar to the shift of the PA-swing predicted for a finite emission height. In addition, the trailing component usually dominates in total power.

The $W_{10} - \dot{E}$ distribution clearly shows sub-groups which are not visible in the pulse $W_{10} - P$ distribution, suggesting that \dot{E} is an important physical parameter for pulsar magnetospheres. Besides a group of pulsars which probably have beams aligned with the rotation axis and a group of pulsars with interpulses which are probably orthogonal rotators there is a group of energetic wide beam pulsars. These young pulsars have very wide profiles with often steep edges which are likely to be emitted from a single pole.

The profile properties of the energetic wide beam pulsars are similar to those of the high energy profiles, suggesting another possible link with the high energy emission. We therefore propose that the emission of these pulsars could come, like the high energies, from extended parts of the magnetosphere. The extended height range from where the emission is emitted will smear out the complex features of the profiles. A large height range could also prevent the emission height to vary much from pulsar to pulsar, which would result in a stronger $W_{10} - P$ correlation for high \dot{E} pulsars, as is indeed observed. If the radio emission and γ -ray emission of these pulsars indeed come from similar locations in the magnetosphere, one would expect the radio and γ -ray profiles to look alike, something that potentially can be tested by the Fermi satellite.

An alternative mechanism to produce the profiles of the energetic wide beam pulsars could be the combination of refraction (or scattering) of radio waves in pulsar magnetospheres with an emission height which is different for different field lines (Weltevrede et al. 2003). Refraction (and scattering) is most severe for the ordinary wave mode, suggesting that these profiles are dominated by one polarization mode. This would be consistent with the high degree of linear polarization observed for these pulsars. The unpolarized bump in the middle of the profiles of the energetic wide beam pulsars could be the un-refracted part of the beam, which is depolarized because the mixing of the plasma modes.

Measurements of the emission height could potentially discriminate between the refraction model and the extended emission height model for the energetic wide beam pulsars. There is no evidence that pulsars with large emission heights (derived from their PA-swing) have wider profiles. It is therefore not clear what the physical meaning of these emission heights are. It could support the idea that the beams of energetic wide beam pulsars are wide because of refraction instead of caused by a large emission heights. However, it could also mean that the emission height of the outer parts of the beam is much larger than for the central parts, making the emission geometry similar to that of a slot gap.

ACKNOWLEDGMENTS

The authors would like to thank the referee, Axel Jessner, for his useful comments on this paper. The Australia Telescope is funded by the Commonwealth of Australia for operation as a National Facility managed by the CSIRO.

REFERENCES

- Barnard J. J., Arons J., 1986, *ApJ*, 302, 138
- Biggs J. D., 1990, *MNRAS*, 245, 514
- Blaskiewicz M., Cordes J. M., Wasserman I., 1991, *ApJ*, 370, 643
- Cheng K. S., Ho C., Ruderman M., 1986, *ApJ*, 300, 500
- Crawford F., Manchester R. N., Kaspi V. M., 2001, *AJ*, 122, 2001
- D'Amico N., Stappers B. W., Bailes M., Martin C. E., Bell J. F., Lyne A. G., Manchester R. N., 1998, *MNRAS*, 297, 28
- Daugherty J. K., Harding A. K., 1996, *ApJ*, 458, 278
- Dyks J., 2008, *astro-ph/0806.0554*
- Dyks J., Frackowiak M., Słowikowska A., Rudak B., Zhang B., 2005, *ApJ*, 633, 1101
- Dyks J., Harding A. K., 2004, *ApJ*, 614, 869
- Dyks J., Rudak B., 2003, *ApJ*, 598, 1201
- Dyks J., Rudak B., Harding A. K., 2004, *ApJ*, 607, 939
- Everett J. E., Weisberg J. M., 2001, *ApJ*, 553, 341
- Gil J. A., Kijak J., Seiradakis J. H., 1993, *A&A*, 272, 268
- Gonthier P. L., Story S. A., Clow B. D., Harding A. K., 2007, *Astrophys. Space Sci.*, 309, 245
- Gould D. M., Lyne A. G., 1998, *MNRAS*, 301, 235
- Gupta Y., Gangadhara R. T., 2003, *ApJ*, 584, 418
- Han J. L., Manchester R. N., Xu R. X., Qiao G. J., 1998, *MNRAS*, 300, 373
- Harding A. K., Muslimov A. G., 2001, *ApJ*, 556, 987
- Harding A. K., Muslimov A. G., 2002, *ApJ*, 568, 862
- Hotan A. W., van Straten W., Manchester R. N., 2004, *Publications of the Astronomical Society of Australia*, 21, 302
- Huguenin G. R., Manchester R. N., Taylor J. H., 1971, *ApJ*, 169, 97
- Johnston S., Hobbs G., Vigeland S., Kramer M., Weisberg J. M., Lyne A. G., 2005, *MNRAS*, 364, 1397
- Johnston S., Kramer M., Karastergiou A., Hobbs G., Ord S., Wallman J., 2007, *MNRAS*, 381, 1625
- Johnston S., Lyne A. G., Manchester R. N., Kniffen D. A., D'Amico N., Lim J., Ashworth M., 1992, *MNRAS*, 255, 401
- Johnston S., Weisberg J. M., 2006, *MNRAS*, 368, 1856
- Karastergiou A., Johnston S., 2007, *MNRAS*, 380, 1678
- Karastergiou A., Johnston S., Manchester R. N., 2005, *MNRAS*, 359, 481
- Keith M. J., Johnston S., Kramer M., Weltevrede P., Waters K. P., Stappers B. W., 2008, *MNRAS*, in press (*astro-ph/0807.2088*)
- Kijak J., Gil J., 1997, *MNRAS*, 288, 631
- Kramer M., Johnston S., 2008, *MNRAS*, in press (*astro-ph/0807.5013*)
- Kramer M., Wielebinski R., Jessner A., Gil J. A., Seiradakis J. H., 1994, *A&AS*, 107, 515
- Kramer M., Xilouris K. M., Lorimer D. R., Doroshenko O., Jessner A., Wielebinski R., Wolszczan A., Camilo F., 1998, *ApJ*, 501, 270
- Lorimer D. R., Kramer M., 2005, *Handbook of Pulsar Astronomy*. Cambridge University Press
- Lyne A. G., Manchester R. N., 1988, *MNRAS*, 234, 477
- Manchester B. N., 1996, in Johnston S., Walker M. A., Bailes M., eds, *ASP Conf. Ser. 105: IAU Colloq. 160: Pulsars: Problems and Progress Wide Beams from Young Pulsars (or One Pole for All)*. pp 193–+
- Manchester R. N., Han J. L., Qiao G. J., 1998, *MNRAS*, 295, 280
- Manchester R. N., Hobbs G. B., Teoh A., Hobbs M., 2005, *AJ*, 129, 1993
- Manchester R. N., Johnston S., 1995, *ApJ*, 441, L65
- Manchester R. N., Lyne A. G., 1977, *MNRAS*, 181, 761
- Manchester R. N., Taylor J. H., Huguenin G. R., 1975, *ApJ*, 196, 83
- Marquardt D., 1963, *Journal of the Society for Industrial and Applied Mathematics*, 11, 431
- Mitra D., Li X. H., 2004, *A&A*, 421, 215
- Mitra D., Rankin J. M., 2002, *ApJ*, 577, 322
- Morini M., 1983, *MNRAS*, 202, 495
- Muslimov A. G., Harding A. K., 2004a, *ApJ*, 606, 1143
- Muslimov A. G., Harding A. K., 2004b, *ApJ*, 617, 471
- Pellizzoni A., Pilia M., Possenti A., Fornari F., Caraveo P., Del Monte E., Mereghetti S., Tavani M., Argan A., Trois e. a., 2008, *ApJ*, submitted
- Petrova S. A., 2008, *MNRAS*, 384, L1
- Press W. H., Teukolsky S. A., Vetterling W. T., Flannery B. P., 1992, *Numerical Recipes: The Art of Scientific Computing*, 2nd edition. Cambridge University Press, Cambridge
- Qiao G. J., Manchester R. N., Lyne A. G., Gould D. M., 1995, *MNRAS*, 274, 572
- Radhakrishnan V., Cooke D. J., 1969, *Astrophys. Lett.*, 3, 225
- Radhakrishnan V., Rankin J. M., 1990, *ApJ*, 352, 258
- Rankin J. M., 1983, *ApJ*, 274, 333
- Rankin J. M., 1993a, *ApJ*, 405, 285
- Rankin J. M., 1993b, *ApJS*, 85, 145
- Romani R. W., 1996, *ApJ*, 470, 469
- Romani R. W., Yadigaroglu I.-A., 1995, *ApJ*, 438, 314
- Smith D., Guillemot L., Camilo F., Cognard I., Dumora D., Espinoza C., et al. 2008, *A&A*, submitted
- Thompson D. J., 2004, in Cheng K. S., Romero G. E., eds, *Cosmic Gamma-Ray Sources Vol. 304 of Astrophysics and Space Science Library, Gamma ray pulsars*. pp 149–+
- van Straten W., 2004, *Astrophys. J. Supp. Series*, 152, 129
- van Hoensbroech A., Lesch H., Kunzl T., 1998, *A&A*, 336, 209
- von Mises R., 1918, *Physikalische Zeitschrift*, 19, 490
- Weisberg J. M., Cordes J. M., Kuan B., Devine K. E., Green J. T., Backer D. C., 2004, *Astrophys. J. Supp. Series*, 150, 317
- Weltevrede P., Johnston S., 2008, *MNRAS*, 387, 1755
- Weltevrede P., Stappers B. W., van den Horn L. J., Edwards R. T., 2003, *A&A*, 412, 473
- Weltevrede P., Wright G. A. E., Stappers B. W., 2007, *A&A*

APPENDIX A: POLARIZATION FIGURES AT BOTH 10 AND 20 CM

The *astro-ph* version is missing 528 figures due to file size restrictions. Please download the paper including the appendices from <http://www.atnf.csiro.au/people/pulsar/wj08b.pdf>.

**APPENDIX B: POLARIZATION FIGURES
ONLY AT 20 CM**

The astro-ph version is missing 528 figures due to file size restrictions. Please download the paper including the appendices from <http://www.atnf.csiro.au/people/pulsar/wj08b.pdf>.

**APPENDIX C: TABLE WITH THE PROFILE
PROPERTIES**

Name	λ_{obs} [cm]	t_{obs} [sec]	Class	S/N	Scat.	W_{50} [$^{\circ}$]	W_{10} [$^{\circ}$]	N_{Comp}	Sym.	L [%]	V [%]	Fig.
J0034-0721	20	959	S	217	N	12.4	34.5	2	0.964	7.8 ± 0.8	3.4 ± 0.5	B1
J0051+0423	20	3838	D	32	N	31.1	42.3		0.926			B1
J0108-1431	10	6565	S	54	N	10.5	26.3		0.978	40.0 ± 3.9		A1
J0108-1431	20	19731	S	186	N	12.2	28.5	2	0.990	71.1 ± 1.1	13.7 ± 0.8	A1
J0134-2937	20	960	D	238	N	5.6	18.2	4	0.803	41.9 ± 0.8	-21.1 ± 0.5	B1
J0151-0635	20	959	D	51	N	29.3	39.0		0.884	22.0 ± 2.5		B1
J0152-1637	20	958	D	506	N	6.8	9.8	3	0.939	12.1 ± 0.3	-2.0 ± 0.2	B1
J0206-4028	20	960	D	52	N	3.5	10.1		0.973		6.9 ± 2.2	B1
J0211-8159	20	1918	S	18	N	20.6	37.6		0.887			B1
J0255-5304	20	960	D	157	N	6.3	8.7	2	0.978	6.5 ± 0.9	-6.3 ± 0.5	B1
J0304+1932	20	959	D	298	N	11.3	15.8	2	0.945	31.5 ± 0.5	13.0 ± 0.4	B1
J0401-7608	10	5455	D	122	N	12.9	17.9	2	0.964	20.6 ± 1.3		A1
J0401-7608	20	7582	M	383	N	13.8	18.0	2	0.989	27.1 ± 0.4		A1
J0448-2749	20	960	S	58	N	9.2	16.7		0.992	19.7 ± 3.6	-14.3 ± 2.6	B1
J0450-1248	20	960	D	50	N	20.5	30.0		0.990	16.7 ± 3.5		B1
J0459-0210	20	958	D	38	N	3.4	13.2		0.890		-9.4 ± 3.1	B1
J0520-2553	20	960	D	51	N	15.1	19.6		0.796	14.0 ± 3.3		B1
J0525+1115	20	959	M	103	N	14.4	17.6	3	0.894	9.2 ± 1.7	6.8 ± 1.2	B1
J0533+0402	20	1918	S	81	N	5.5	10.1		0.996	7.9 ± 2.4		B1
J0536-7543	10	3567	M	118	N	16.6	25.3	3	0.918	29.3 ± 1.4	-23.2 ± 1.0	A1
J0536-7543	20	10775	M	1557	N	17.0	27.0	4	0.899	47.5 ± 0.1	-11.1 ± 0.1	A1
J0540-7125	20	1916	M	29	N	9.6	15.9		0.895			B1
J0543+2329	20	809	D	194	N	7.8	23.3	2	0.971	43.2 ± 1.0	-8.9 ± 0.7	B1
J0601-0527	20	960	D	138	N	16.1	21.8	2	0.888	28.8 ± 1.1	2.9 ± 0.8	B1
J0614+2229	10	180	S	47	N	8.0	14.6		0.983	46.3 ± 3.8	16.8 ± 2.8	A1
J0614+2229	20	807	S	197	N	7.4	13.5	1	0.997	69.8 ± 0.9	18.5 ± 0.6	A1
J0624-0424	20	899	M	167	N	2.0	21.9	4	0.736	21.7 ± 0.8	6.4 ± 0.6	B1
J0630-2834	10	2396	S	297	N	16.3	30.5	3	0.998	24.5 ± 0.6	-4.2 ± 0.4	A1
J0630-2834	20	5776	S	871	N	18.4	34.9	3	0.999	44.8 ± 0.2	-3.3 ± 0.1	A1
J0631+1036	20	1919	M	78	N	8.2	24.4		0.987	82.6 ± 2.2		B1
J0636-4549	20	1917	S	20	N	3.2	5.9		0.973			B2
J0656-2228	20	900	S	50	N	4.7	8.7		0.985			B2
J0656-5449	20	960	S	30	N	10.9	20.0		0.939		-17.9 ± 5.3	B2
J0659+1414	10	179	S	87	N	14.8	32.1		0.986	49.7 ± 2.3	-14.5 ± 1.7	A1
J0659+1414	20	717	S	111	N	13.9	30.3	1	0.984	70.5 ± 1.7	-15.0 ± 1.2	A1
J0709-5923	20	959	S	26	N	4.1	7.5		0.966			B2
J0719-2545	20	959	S	62	N	6.2	11.3		0.917	10.0 ± 2.9	13.6 ± 2.1	B2
J0729-1448	10	1779	D	34	N	20.0	28.0		0.946	78.9 ± 5.4		A1
J0729-1448	20	5146	D	94	N	10.7	26.7		0.886	72.1 ± 1.9	16.6 ± 1.2	A1
J0729-1836	20	960	D	88	N	9.8	18.5		0.896	19.6 ± 2.1	-6.1 ± 1.5	B2
J0742-2822	10	430	M	448	N	9.9	16.0	3	0.961	80.6 ± 0.4	-4.2 ± 0.3	A1
J0742-2822	20	3296	M	2463	N	9.9	15.9	3	0.972	81.4 ± 0.1	-1.7 ± 0.0	A1
J0745-5353	10	2079	S	96	N	17.7	32.4		0.992	11.9 ± 1.8		A1
J0745-5353	20	10012	S	476	N	18.2	33.6	2	0.997	20.8 ± 0.4	3.6 ± 0.3	A1
J0749-4247	20	959	S	44	N	4.8	8.8		0.963	17.9 ± 4.1		B2
J0820-3921	20	1920	S	26	N	24.2	44.4		0.941	23.2 ± 6.2	15.5 ± 4.2	B2
J0821-3824	20	1079	S	30	N	17.1	31.2		0.934			B2
J0821-4221	20	960	D	43	N	13.8	22.5		0.933			B2
J0834-4159	10	3580	S	15	N	10.8	20.3		0.875			A1
J0834-4159	20	15737	S	59	N	13.3	23.4		0.965		-11.7 ± 2.3	A1
J0834-4159I	20	15737	S	17	N	15.5	28.4		0.907			A1
J0835-4510	10	820	D	9275	N	6.4	17.2	4	0.833	89.6 ± 0.0	-17.5 ± 0.0	A2
J0835-4510	20	6496	D	26906	N	6.0	14.3	3	0.949	90.0 ± 0.0	-6.0 ± 0.0	A2
J0838-2621	20	1919	D	31	N	10.0	35.2		0.886			B2
J0843-5022	20	960	S	36	N	10.2	18.7		0.968			B2
J0849-6322	20	1919	D	68	N	6.5	22.7		0.900	24.8 ± 2.6	-9.1 ± 1.7	B2
J0855-4644	10	3560	S	12	N	38.0	70.1		0.796			A2
J0855-4644	20	29519	S	49	N	35.5	65.4		0.953	48.0 ± 3.8		A2
J0856-6137	20	959	S	94	N	7.6	13.8		0.997	8.9 ± 1.9	5.3 ± 1.4	B2

Table C1. The measured profile properties of the sample of pulsars. The first column is the pulsar name (I indicates the interpulse), followed by the observing wavelength, the total integration time, the classification (Single, Double or Multiple), the signal to noise ratio of the profile, whether the profile shows some evidence for scattering (by eye), the profile width measured at the 50% intensity point, the profile width measured at the 10% intensity point, the number of significant fit functions to the profile for a S/N of 30, the symmetry coefficient, the percentage linear polarization, the percentage circular polarization and the figure number.

Name	λ_{obs} [cm]	t_{obs} [sec]	Class	S/N	Scat.	W_{50} [°]	W_{10} [°]	N_{Comp}	Sym.	L [%]	V [%]	Fig.
J0857-4424	10	669	S	19	N	9.6	17.5		0.956			A2
J0857-4424	20	3493	S	110	N	11.0	18.8	2	0.989			A2
J0901-4624	10	1389	M	24	N	3.1	18.2		0.755	51.1 ± 6.7	-44.1 ± 4.6	A2
J0901-4624	20	4242	M	48	N	3.2	26.9		0.862	53.3 ± 3.8	-35.5 ± 2.7	A2
J0902-6325	20	959	S	110	N	9.5	16.3	2	0.970	24.0 ± 1.8	7.3 ± 1.2	B2
J0905-4536	20	960	S	28	N	54.1	86.0		0.849			B2
J0905-5127	10	2309	D	19	N	9.7	13.9		0.949	51.1 ± 9.5	23.1 ± 6.7	A2
J0905-5127	20	3043	D	137	N	9.0	12.3	2	0.997	73.5 ± 1.2	11.0 ± 0.8	A2
J0905-5127I	20	3043	S	14	N	3.8	7.0		0.836			A2
J0907-5157	20	960	M	396	N	18.2	33.6	3	0.872	32.7 ± 0.4	3.8 ± 0.3	B2
J0908-4913	10	460	D	497	N	3.0	10.9	2	0.929	93.5 ± 0.3	-4.4 ± 0.3	A2
J0908-4913I	10	460	D	131	N	13.8	16.4	2	0.776	90.0 ± 1.3		A2
J0908-4913	20	9638	D	1841	N	3.6	11.7	2	0.914	90.0 ± 0.1	4.1 ± 0.1	A2
J0908-4913I	20	9638	D	460	N	13.3	17.1	2	0.840	87.4 ± 0.3	-1.3 ± 0.2	A2
J0924-5302	20	959	D	95	N	6.1	11.1		0.889	19.3 ± 1.9		B2
J0924-5814	20	959	S	117	N	22.4	41.1	1	0.993	45.2 ± 1.7		B2
J0932-3217	20	958	S	44	N	2.9	5.4		0.977			B2
J0934-4154	20	959	S	23	N	6.8	15.9		0.850			B3
J0940-5428	10	940	D	15	N	15.1	42.1		0.779	34.9 ± 10.9		A2
J0940-5428	20	4358	D	58	N	12.2	38.5		0.832	52.2 ± 2.8		A2
J0941-5244	20	960	D	36	N	9.4	13.9		0.912			B3
J0942-5657	20	959	D	186	N	2.4	6.0	2	0.975	37.9 ± 0.8	10.1 ± 0.6	B3
J0954-5430	10	1419	D	62	N	2.5	10.2		0.934	31.4 ± 2.7	8.2 ± 2.0	A2
J0954-5430	20	3003	D	65	N	3.4	13.4		0.894	39.0 ± 2.7	15.6 ± 1.8	A2
J1003-4747	10	940	S	24	N	10.8	19.7		0.926	20.7 ± 6.7		A3
J1003-4747	20	2985	D	125	N	7.8	21.4	2	0.984	10.5 ± 1.3	2.6 ± 0.9	A3
J1012-5857	20	959	S	107	N	3.3	9.1	2	0.994	6.1 ± 1.6	5.4 ± 1.2	B3
J1015-5719	10	700	D	77	N	76.4	115.7		0.942	71.6 ± 2.9	-12.7 ± 2.0	A3
J1015-5719	20	2317	M	93	N	113.7	150.6		0.961	61.1 ± 1.8	-13.5 ± 1.3	A3
J1016-5345	20	960	S	34	N	3.8	6.9		0.986			B3
J1016-5819	20	9758	S	49	N	12.4	22.7		0.974			B3
J1016-5857	10	460	S	26	N	7.4	13.6		0.894	70.6 ± 7.9		A3
J1016-5857	20	2468	D	59	N	11.0	39.6		0.891	52.6 ± 2.9	11.4 ± 2.1	A3
J1017-5621	20	960	S	81	N	2.7	9.9		0.953	11.7 ± 1.3	-16.6 ± 0.9	B3
J1019-5749	10	820	S	132	N	12.9	31.2	2	0.947	33.3 ± 1.5		A3
J1019-5749	20	4237	S	69	Y	102.7	226.3		0.835	24.9 ± 1.4		A3
J1020-6026	10	1800	S	12	N	30.1	55.1		0.716			A3
J1020-6026	20	8099	S	28	N	45.3	83.8		0.924			A3
J1028-5819	10	960	D	49	N	0.8	2.5		0.916	92.2 ± 3.3		A3
J1028-5819	20	3179	D	33	N	0.8	2.5		0.945	63.5 ± 5.5		A3
J1032-5911	20	960	S	39	N	14.8	27.1		0.951			B3
J1034-3224	20	958	M	133	N	79.1	95.0	5	0.849	15.9 ± 1.5	5.2 ± 1.0	B3
J1036-4926	20	960	D	52	N	3.3	12.3		0.872	18.6 ± 3.6		B3
J1038-5831	20	959	D	46	N	3.1	11.8		0.854	20.5 ± 3.5		B3
J1043-6116	10	820	M	58	N	2.6	14.2		0.847		-13.4 ± 2.2	A3
J1043-6116	20	2405	M	166	N	5.7	13.4	2	0.868	7.1 ± 1.0	-7.8 ± 0.7	A3
J1046-5813	20	959	D	99	N	8.7	12.2		0.936	11.6 ± 1.6		B3
J1047-3032	20	960	S	37	N	26.3	48.1		0.976			B3
J1047-6709	20	960	S	129	N	3.9	19.2	3	0.898	66.8 ± 1.4	-13.4 ± 1.0	B3
J1048-5832	10	580	M	374	N	5.3	21.5	4	0.949	80.3 ± 0.4	10.0 ± 0.3	A3
J1048-5832	20	3727	M	825	N	15.5	26.4	3	0.920	67.8 ± 0.2	7.6 ± 0.1	A3
J1052-5954	10	3579	S	15	N	6.4	11.6		0.868	59.3 ± 11.0		A3
J1052-5954	20	19596	S	26	N	10.8	19.8		0.946	47.4 ± 6.0		A3
J1055-6032	10	1440	S	18	N	13.2	24.2		0.940			A3
J1055-6032	20	2669	S	17	N	16.7	30.4		0.861			A3
J1057-5226	10	820	M	50	N	23.3	34.9		0.726	83.6 ± 3.5		A4
J1057-5226I	10	820	M	46	N	12.9	34.6		0.853	39.5 ± 4.7		A4
J1057-5226	20	20195	M	359	N	24.1	33.2	4	0.779	91.3 ± 0.5	6.3 ± 0.3	A4
J1057-5226I	20	20195	M	325	N	15.0	44.0	2	0.875	38.1 ± 0.6		A4
J1105-6107	10	1780	D	41	N	16.0	21.0		0.873	79.1 ± 3.9	14.7 ± 2.8	A4
J1105-6107	20	5409	D	94	N	17.8	22.5		0.986	77.0 ± 1.7	8.1 ± 1.3	A4
J1110-5637	20	960	D	92	N	13.5	17.3		0.916	22.2 ± 1.2	-7.5 ± 0.8	B3
J1112-6103	10	580	D	67	N	19.6	28.2		0.857	71.8 ± 2.7		A4
J1112-6103	20	3669	S	78	Y	36.5	132.5		0.801	18.4 ± 2.2		A4

Table C1. continued.

Name	λ_{obs} [cm]	t_{obs} [sec]	Class	S/N	Scat.	W_{50} [°]	W_{10} [°]	N_{Comp}	Sym.	L [%]	V [%]	Fig.
J1112-6613	20	960	D	93	N	15.3	22.4		0.955	10.4 ± 1.8	8.5 ± 1.3	B3
J1112-6926	20	959	D	64	N	11.3	16.4		0.970			B3
J1114-6100	20	959	S	141	N	11.8	21.0	2	0.977			B3
J1115-6052	10	879	S	22	N	6.7	12.2		0.902			A4
J1115-6052	20	2995	S	48	N	6.1	11.2		0.945	45.4 ± 4.4		A4
J1119-6127	10	1149	S	32	N	19.3	35.3		0.935	77.7 ± 5.4	-13.0 ± 3.6	A4
J1119-6127	20	14667	S	101	N	20.0	46.0	2	0.989	76.8 ± 1.7	12.0 ± 1.1	A4
J1123-4844	20	960	D	162	N	12.6	19.5	2	0.877	26.4 ± 1.1	27.5 ± 0.8	B3
J1123-6259	10	1300	S	9	N	7.8	14.3		0.839			A4
J1123-6259	20	4956	S	71	N	9.0	16.3		0.984	36.8 ± 2.8		A4
J1126-6054	20	960	S	89	N	7.9	14.5		0.985	13.1 ± 2.3	7.7 ± 1.7	B3
J1126-6054I	20	960	S	7	N	3.2	6.0		0.949			B3
J1126-6942	20	899	S	22	N	7.3	13.4		0.973			B4
J1133-6250	20	958	M	137	N	91.8	113.0	3	0.956	11.4 ± 1.5	3.5 ± 1.0	B4
J1137-6700	20	1918	D	50	N	56.3	83.3		0.901	14.2 ± 2.9		B4
J1138-6207	10	700	S	31	N	6.3	11.4		0.970	53.7 ± 6.9	39.1 ± 5.2	A4
J1138-6207	20	4588	S	42	Y	20.8	73.4		0.787	36.8 ± 4.4	27.4 ± 2.9	A4
J1141-3107	20	960	D	50	N	13.7	19.1		0.959	16.5 ± 3.4	9.8 ± 2.4	B4
J1141-3322	20	1919	M	144	N	13.8	26.1	3	0.990	34.6 ± 1.1	-12.5 ± 0.7	B4
J1143-5158	20	959	S	26	N	5.0	9.1		0.970			B4
J1146-6030	20	960	M	155	N	14.5	18.4	3	0.992	21.1 ± 1.0	3.6 ± 0.8	B4
J1156-5707	10	1109	S	15	N	4.1	7.4		0.921			A4
J1156-5707	20	5045	D	42	N	3.8	15.9		0.940	28.6 ± 4.6		A4
J1204-6843	20	960	D	37	N	9.5	13.4		0.975		-11.9 ± 3.1	B4
J1215-5328	20	959	D	22	N	20.6	28.3		0.904			B4
J1216-6223	10	2079	S	8	N	15.6	28.5		0.704			A4
J1216-6223	20	12543	S	36	N	11.5	21.1		0.980		20.2 ± 3.7	A4
J1224-6407	10	579	D	290	N	9.3	13.8	3	0.811	20.4 ± 0.6	16.3 ± 0.4	A5
J1224-6407	20	2766	D	947	N	9.4	14.0	2	0.967	27.4 ± 0.2	26.0 ± 0.1	A5
J1225-5556	20	958	D	22	N	7.0	10.6		0.909			B4
J1225-6408	20	960	D	95	N	4.8	19.2		0.909	27.4 ± 1.8		B4
J1231-4609	20	960	D	86	N	17.6	24.9		0.967	27.1 ± 1.9	-22.1 ± 1.4	B4
J1236-5033	20	960	S	28	N	14.9	27.2		0.922		-13.4 ± 4.3	B4
J1240-4124	20	959	S	37	N	3.9	7.1		0.921			B4
J1244-5053	20	1919	S	19	N	7.4	13.6		0.945			B4
J1248-6344	20	13087	S	24	N	23.2	42.4		0.930			B4
J1253-5820	20	960	S	198	N	5.5	16.7	2	0.994	56.7 ± 0.9	7.0 ± 0.6	B4
J1301-6305	10	1740	S	17	N	37.6	69.3		0.806	69.9 ± 11.5		A5
J1301-6305	20	13418	S	44	N	47.3	87.7		0.944	69.5 ± 4.6	-15.5 ± 3.5	A5
J1302-6350	20	5189	D	131	N	176.9	211.6	5	0.937	63.4 ± 1.4	19.4 ± 0.9	A5
J1305-6203	10	939	S	20	N	10.7	19.5		0.897			A5
J1305-6203	20	3545	S	57	N	12.6	22.9		0.975	24.3 ± 3.2		A5
J1305-6455	20	959	S	91	N	10.2	32.3		0.954	31.5 ± 4.7	14.8 ± 3.5	B4
J1306-6617	20	959	D	189	N	15.7	41.3	2	0.952	15.2 ± 0.9	7.9 ± 0.7	B4
J1319-6056	20	960	D	86	N	6.0	14.8		0.950	29.3 ± 2.0	-8.6 ± 1.4	B4
J1320-3512	20	960	S	191	N	7.7	23.0	2	0.973	24.0 ± 0.9	12.6 ± 0.6	B5
J1320-5359	10	459	S	35	N	11.0	20.0		0.967			A5
J1320-5359	20	2165	S	182	N	10.2	18.7	1	0.996	18.9 ± 1.0	-5.9 ± 0.7	A5
J1326-5859	20	959	D	361	Y	4.5	16.2	3	0.989	32.8 ± 0.2	4.8 ± 0.1	B5
J1327-6301	20	1920	D	214	N	9.1	41.5	3	0.967	23.0 ± 1.1		B5
J1327-6400	10	2499	S	9	N	11.1	20.3		0.657			A5
J1327-6400	20	7386	S	24	N	18.4	33.6		0.897			A5
J1333-4449	20	960	D	14	N	1.9	10.0		0.736			B5
J1338-6204	20	959	D	188	Y	26.9	42.3	2	0.964	21.5 ± 1.0	9.1 ± 0.7	B5
J1339-4712	20	960	S	54	N	4.9	9.0		0.964	13.9 ± 3.2	-26.0 ± 2.3	B5
J1340-6456	20	960	S	43	N	12.8	23.3		0.955		-16.9 ± 3.6	B5
J1341-6220	10	460	S	89	N	4.2	13.8		0.975	80.2 ± 2.1	-11.8 ± 1.6	A5
J1341-6220	20	2587	S	120	Y	14.2	39.2	2	0.904	52.5 ± 1.5	-15.4 ± 1.1	A5
J1349-6130	10	460	S	27	N	5.9	10.8		0.943	23.6 ± 6.8		A5
J1349-6130	20	2435	S	62	N	7.4	13.5		0.989	24.8 ± 2.7		A5
J1352-6803	20	960	S	66	N	15.3	23.6		0.962	34.9 ± 2.9	-10.0 ± 2.2	B5
J1356-5521	20	1919	S	91	N	12.8	23.4		0.991	22.8 ± 2.1		B5
J1357-6429	10	1749	S	16	N	31.6	58.1		0.895	57.6 ± 12.1	-31.0 ± 8.3	A5
J1357-6429	20	6847	S	45	N	36.9	68.0		0.961	56.4 ± 3.8	-11.4 ± 2.8	A5

Table C1. continued.

Name	λ_{obs} [cm]	t_{obs} [sec]	Class	S/N	Scat.	W_{50} [°]	W_{10} [°]	N_{Comp}	Sym.	L [%]	V [%]	Fig.
J1359-6038	10	460	S	153	N	8.5	14.3	1	0.993	64.3 ± 1.2	17.8 ± 0.9	A5
J1359-6038	20	3548	S	1068	N	7.2	14.0	2	0.998	70.5 ± 0.2	17.8 ± 0.1	A5
J1403-7646	20	899	D	31	N	26.9	40.5		0.837			B5
J1406-6121	10	1420	S	45	N	3.8	7.1		0.995		-65.9 ± 2.3	A6
J1406-6121	20	7866	S	30	Y	15.3	46.0		0.877		-42.3 ± 3.8	A6
J1410-6132	10	2580	S	202	N	12.7	27.4	3	0.938	47.8 ± 1.0		A6
J1410-6132	20	9149	S	53	Y	131.0	233.5		0.896	21.9 ± 1.8		A6
J1410-7404	20	960	S	89	N	1.6	4.3		0.954	15.3 ± 1.8	44.2 ± 0.9	B5
J1412-6145	10	699	S	17	N	7.7	14.1		0.926	39.4 ± 9.9		A6
J1412-6145	20	3664	S	41	N	12.5	22.8		0.935	26.2 ± 4.2	17.5 ± 3.1	A6
J1413-6141	10	939	S	60	N	3.6	6.5		0.992			A6
J1413-6141	20	10832	S	63	Y	17.2	51.2		0.926			A6
J1413-6307	20	960	S	77	N	3.0	7.2		0.945	18.2 ± 2.2	5.3 ± 1.4	B5
J1415-6621	20	960	S	36	N	7.1	12.9		0.987			B5
J1420-6048	10	1240	D	64	N	39.9	51.2		0.870	74.1 ± 2.9	-24.2 ± 2.2	A6
J1420-6048	20	6909	D	81	N	45.1	63.2		0.810	70.1 ± 1.9	-18.8 ± 1.3	A6
J1427-4158	20	1919	D	31	N	10.1	15.3		0.965			B5
J1452-5851	10	1689	S	15	N	10.4	18.9		0.889	58.5 ± 11.1	-31.8 ± 8.8	A6
J1452-5851	20	6604	S	42	N	9.5	17.4		0.970	54.8 ± 4.0	-25.0 ± 3.0	A6
J1452-6036	10	690	D	95	N	2.0	3.6		0.958	24.6 ± 3.5		A6
J1452-6036	20	2108	D	116	N	3.8	31.2	4	0.871	31.0 ± 1.7	-6.9 ± 1.2	A6
J1453-6413	10	460	S	153	N	9.4	19.8	3	0.941	24.0 ± 1.2	-2.9 ± 0.8	A6
J1453-6413	20	2167	M	1159	N	6.4	16.4	4	0.990	26.5 ± 0.2	6.6 ± 0.1	A6
J1456-6843	10	599	S	350	N	15.1	32.1	2	0.981	8.0 ± 0.5		A6
J1456-6843	20	3567	M	2127	N	17.8	34.5	3	0.989	10.5 ± 0.1	4.7 ± 0.1	A6
J1507-4352	20	960	S	59	N	5.9	10.7		0.982	21.0 ± 2.9	-7.8 ± 1.9	B5
J1507-6640	20	960	S	58	N	3.2	5.9		0.979		8.6 ± 2.0	B5
J1509-5850	20	11289	S	23	N	18.8	34.4		0.911	24.2 ± 8.0		B5
J1512-5759	10	540	S	77	N	12.1	22.1		0.992			A6
J1512-5759	20	2228	S	440	N	13.8	28.5	2	0.973	7.0 ± 0.4		A6
J1513-5908	10	1710	S	20	N	62.4	117.5		0.777	54.4 ± 9.0		A7
J1513-5908	20	5317	S	62	N	36.0	66.4		0.975	64.2 ± 2.7	-18.6 ± 1.9	A7
J1514-4834	20	419	D	66	N	6.2	10.5		0.871		-6.6 ± 1.9	B5
J1514-5925	10	2129	S	30	N	2.6	5.2		0.939	81.9 ± 5.5		A7
J1514-5925	20	8588	S	34	N	11.0	20.2		0.949	64.0 ± 5.3		A7
J1515-5720	20	6756	D	31	N	10.1	18.9		0.945			A7
J1517-4356	20	959	S	35	N	6.2	11.4		0.976			B5
J1522-5829	20	960	S	232	N	12.9	24.0	2	0.952	26.6 ± 0.7	3.2 ± 0.5	B5
J1524-5625	10	1560	D	36	N	45.6	69.0		0.883	45.6 ± 5.0		A7
J1524-5625	20	4869	D	71	N	17.1	69.3		0.855	57.2 ± 2.3		A7
J1524-5706	10	497	S	10	N	9.5	17.3		0.818			A7
J1524-5706	20	1924	S	38	N	5.2	9.6		0.989	24.3 ± 5.0	11.4 ± 3.1	A7
J1528-4109	20	359	S	24	N	5.7	10.4		0.915			B6
J1530-5327	10	689	D	31	N	5.2	14.8		0.836		-12.7 ± 3.8	A7
J1530-5327	20	2135	D	69	N	10.7	16.1		0.875	10.6 ± 2.4	6.1 ± 1.7	A7
J1531-4012	20	959	S	27	N	7.8	14.3		0.970		-22.5 ± 4.9	B6
J1531-5610	10	600	D	37	N	22.9	30.1		0.929	60.4 ± 4.8	20.5 ± 3.3	A7
J1531-5610	20	4588	D	63	N	22.7	31.5		0.844	70.9 ± 2.4	21.3 ± 1.7	A7
J1534-5405	20	960	D	60	N	5.9	25.0		0.971	10.3 ± 3.1	6.6 ± 2.2	B6
J1535-4114	20	959	D	141	N	12.7	18.3	2	0.901	43.9 ± 1.1	7.2 ± 0.7	B6
J1536-3602	20	958	M	90	N	22.5	27.5		0.955	19.7 ± 2.0	-4.4 ± 1.4	B6
J1538-5551	10	2120	S	19	N	3.4	6.3		0.925			A7
J1538-5551	20	9578	S	33	Y	16.5	62.9		0.817		17.0 ± 3.8	A7
J1539-5626	10	459	D	127	N	11.3	21.9	2	0.915	31.1 ± 1.4		A7
J1539-5626	20	1956	D	313	N	11.7	23.9	2	0.932	25.9 ± 0.6	4.4 ± 0.4	A7
J1541-5535	10	1179	S	23	N	4.4	8.0		0.971	22.6 ± 7.5	20.8 ± 5.2	A7
J1541-5535	20	4985	S	30	N	7.7	14.1		0.936	30.0 ± 5.4		A7
J1542-5034	20	959	S	26	N	3.6	6.6		0.957			B6
J1543-5459	10	749	S	26	N	3.2	5.9		0.977	33.4 ± 7.6	33.0 ± 5.2	A8
J1543-5459	20	2643	S	52	Y	8.8	28.1		0.849		33.6 ± 2.7	A8
J1548-5607	10	700	D	21	N	6.2	30.4		0.701	59.9 ± 9.7		A8
J1548-5607	20	1987	D	78	N	11.8	32.3		0.941	50.9 ± 2.0	13.0 ± 1.5	A8
J1549-4848	10	630	S	25	N	9.2	16.8		0.933			A8
J1549-4848	10	630	S	10	N	8.9	16.3		0.799			A8

Table C1. continued.

Name	λ_{obs} [cm]	t_{obs} [sec]	Class	S/N	Scat.	W_{50} [$^{\circ}$]	W_{10} [$^{\circ}$]	N_{Comp}	Sym.	L [%]	V [%]	Fig.
J1549-4848	20	7715	S	100	N	9.0	13.7	1	0.977	13.0 ± 1.8		A8
J1549-4848I	20	7715	S	38	N	10.1	18.4		0.951	25.0 ± 5.1		A8
J1551-5310	10	969	S	26	N	6.7	12.5		0.974		22.7 ± 6.1	A8
J1551-5310	20	4533	S	44	Y	24.8	75.3		0.829		14.1 ± 3.0	A8
J1557-4258	20	960	M	116	N	4.6	19.0	2	0.975	23.0 ± 1.4	-12.3 ± 0.9	B6
J1600-5044	10	460	D	331	N	6.3	9.2	3	0.983	16.5 ± 0.5	22.6 ± 0.4	A8
J1600-5044	20	1867	S	1150	Y	8.3	16.7	3	0.974	13.8 ± 0.2	27.4 ± 0.1	A8
J1600-5751	10	610	S	19	N	32.9	60.6		0.831			A8
J1600-5751	20	2197	M	118	N	18.7	44.3	3	0.968	9.7 ± 1.3	4.3 ± 0.9	A8
J1601-5335	20	5226	S	24	N	10.3	18.8		0.935	37.6 ± 7.4		B6
J1602-5100	10	1358	D	166	N	8.6	13.1	5	0.857	14.8 ± 1.0	5.5 ± 0.7	A8
J1602-5100	20	2035	D	501	N	1.8	10.9	4	0.821	17.2 ± 0.4	7.2 ± 0.3	A8
J1603-3539	20	960	D	35	N	28.5	37.0		0.886			B6
J1603-5657	20	959	S	47	N	2.5	4.6		0.981	32.4 ± 2.9	15.8 ± 1.5	B6
J1605-5257	20	959	D	394	N	33.8	44.4	3	0.884	34.2 ± 0.4	4.7 ± 0.3	B6
J1609-1930	20	958	S	37	N	3.4	6.1		0.980			B6
J1611-5209	10	559	D	58	N	1.5	5.9		0.835	13.3 ± 3.3		A8
J1611-5209	20	2077	D	109	N	2.2	5.5	2	0.922	11.8 ± 1.7	3.7 ± 1.1	A8
J1611-5209I	20	2077	S	0	N	7.6	13.8		0.817			A8
J1612-2408	20	1738	D	42	N	3.6	12.7		0.820			B6
J1614-3937	20	1739	D	44	N	14.4	20.0		0.948	15.5 ± 3.5	-14.3 ± 2.5	B6
J1614-5048	10	790	D	59	N	4.9	15.5		0.910	75.8 ± 3.0	21.8 ± 2.1	A9
J1614-5048	20	3425	S	162	Y	14.0	47.7	2	0.916	55.0 ± 1.2	25.0 ± 0.8	A9
J1615-5537	20	959	D	54	N	2.6	10.7		0.801		10.2 ± 2.2	B6
J1617-5055	10	5880	S	33	N	11.9	21.8		0.980	63.6 ± 4.8	31.1 ± 3.1	A9
J1617-5055	20	33438	S	24	Y	53.3	99.4		0.843		41.5 ± 3.5	A9
J1626-4807	10	2130	S	29	N	18.6	34.1		0.971			A9
J1626-4807	20	19505	S	32	Y	70.2	133.3		0.835			A9
J1627-4706	20	6239	S	19	Y	20.5	37.5		0.816			B6
J1630-4733	20	960	S	122	Y	49.7	134.1	3	0.822	26.2 ± 1.6	-19.8 ± 1.1	B6
J1632-4757	10	2440	D	33	N	14.1	17.7		0.895			A9
J1632-4757	20	11856	S	37	Y	30.5	55.9		0.900			A9
J1632-4818	10	2259	D	18	N	8.8	12.1		0.948	39.7 ± 10.1		A9
J1632-4818	20	10529	S	34	Y	20.0	36.6		0.931	22.9 ± 5.0	16.1 ± 2.9	A9
J1633-4453	20	960	S	107	Y	6.4	17.6	2	0.933	11.0 ± 1.6		B6
J1633-5015	20	960	S	216	N	6.7	16.9	2	0.989	25.8 ± 0.6	-11.2 ± 0.4	B6
J1637-4553	10	700	S	32	N	9.3	16.9		0.967	63.3 ± 6.8		A9
J1637-4553	20	2228	S	100	N	9.9	18.0	1	0.994	72.7 ± 1.9		A9
J1637-4553I	20	2228	S	11	N	13.3	24.3		0.828			A9
J1637-4642	10	1120	S	34	N	26.4	48.4		0.925	69.2 ± 6.6		A9
J1637-4642	20	4278	S	47	N	33.6	61.8		0.966	48.7 ± 4.4	14.1 ± 2.8	A9
J1638-4417	10	2140	S	11	N	14.4	26.3		0.837	64.8 ± 17.2	-40.0 ± 12.9	A9
J1638-4417	20	6038	S	31	N	15.2	27.8		0.928	47.1 ± 6.3		A9
J1638-4608	10	2439	S	34	N	2.7	5.0		0.971	51.4 ± 5.7	-13.1 ± 4.0	A9
J1638-4608	20	5375	S	49	Y	5.7	15.7		0.913	43.7 ± 4.2		A9
J1638-4725	10	2697	S	63	N	12.3	22.4		0.984			A10
J1638-4725	20	4764	S	44	Y	31.5	57.8		0.916			A10
J1639-4604	20	960	S	35	N	9.7	24.2		0.867	18.4 ± 6.1		B6
J1640-4715	10	459	D	42	N	5.2	15.4		0.961			A10
J1640-4715	20	1981	S	67	Y	16.0	38.3		0.944	11.8 ± 3.1		A10
J1641-2347	20	1917	M	121	N	17.0	23.6	3	0.980	43.0 ± 1.3		B7
J1643-4505	10	420	S	18	N	8.3	15.2		0.910		-38.2 ± 6.8	A10
J1643-4505	20	4558	S	36	N	12.3	22.4		0.979		-40.4 ± 3.3	A10
J1646-4346	10	459	S	28	N	8.8	16.1		0.965	32.6 ± 6.5		A10
J1646-4346	20	2106	S	66	Y	19.8	51.7		0.911	27.6 ± 3.1		A10
J1648-4611	10	1110	D	38	N	15.3	19.4		0.965	73.1 ± 4.0	-30.3 ± 2.5	A10
J1648-4611	20	5197	S	45	N	27.9	51.2		0.947	45.8 ± 4.3	-19.1 ± 3.0	A10
J1649-4653	10	1168	S	15	N	6.2	11.3		0.838			A10
J1649-4653	20	5071	S	32	Y	8.8	21.5		0.891			A10
J1649-5553	20	960	S	39	N	37.8	69.7		0.966			B7
J1650-1654	20	959	S	69	N	9.7	13.7		0.991	14.4 ± 2.5		B7
J1650-4502	10	419	S	21	N	3.1	5.7		0.977	65.9 ± 8.3	26.5 ± 5.8	A10
J1650-4502	20	1954	S	41	Y	6.0	11.0		0.946	64.2 ± 4.1		A10
J1650-4921	10	600	D	37	N	5.9	8.2		0.935	38.2 ± 4.9	31.9 ± 3.6	A10

Table C1. continued.

Name	λ_{obs} [cm]	t_{obs} [sec]	Class	S/N	Scat.	W_{50} [°]	W_{10} [°]	N_{Comp}	Sym.	L [%]	V [%]	Fig.
J1650-4921	20	959	S	22	N	6.0	10.9		0.920		19.2 ± 5.8	A10
J1651-7642	20	958	D	47	N	15.9	22.4		0.930	40.9 ± 4.3		B7
J1652-1400	20	960	S	20	N	13.9	25.3		0.933	37.7 ± 8.4	-25.9 ± 6.1	B7
J1653-3838	20	960	D	109	N	3.7	14.8	2	0.860	29.3 ± 1.5	4.3 ± 1.1	B7
J1654-2713	20	959	S	22	N	6.7	12.2		0.967			B7
J1655-3048	20	1919	M	89	N	55.8	73.2		0.928	18.2 ± 1.9	11.3 ± 1.5	B7
J1700-3312	20	959	S	93	N	7.9	14.3		0.945	27.1 ± 1.8	-13.7 ± 1.2	B7
J1701-3726	20	957	D	236	N	6.3	15.7	2	0.901	28.4 ± 0.7	-17.8 ± 0.5	B7
J1701-4533	20	959	D	102	N	20.4	34.7	2	0.977	20.4 ± 1.8	8.4 ± 1.4	B7
J1702-4128	10	1710	S	69	N	11.2	26.9		0.974	76.1 ± 2.5	-9.4 ± 1.7	A10
J1702-4128	20	5497	S	73	Y	21.9	55.4		0.930	43.7 ± 3.1		A10
J1702-4305	20	3808	S	32	N	12.6	23.0		0.943			B7
J1702-4310	10	979	S	29	N	16.8	30.8		0.986	73.7 ± 6.5		A10
J1702-4310	20	3846	S	62	N	17.8	32.5		0.987	67.9 ± 2.8	22.1 ± 2.1	A10
J1703-4851	20	958	M	70	N	7.8	16.5		0.932	15.4 ± 2.3		B7
J1705-1906	10	569	D	120	N	11.0	16.2	2	0.980	37.8 ± 1.4	-6.6 ± 1.0	A11
J1705-1906I	10	569	S	25	N	2.4	4.3		0.938	88.1 ± 6.2		A11
J1705-1906	20	2855	D	718	N	10.2	16.9	2	0.984	39.4 ± 0.2	-11.7 ± 0.2	A11
J1705-1906I	20	2855	S	196	N	2.5	5.7	1	0.987	70.0 ± 0.8	-16.9 ± 0.5	A11
J1705-3950	10	1049	D	79	N	19.1	26.6		0.736	75.8 ± 2.5	-25.1 ± 1.7	A11
J1705-3950	20	2944	D	89	N	25.7	36.5		0.785	60.9 ± 2.2	-22.9 ± 1.4	A11
J1707-4053	20	959	S	177	Y	20.0	54.6	3	0.879	15.0 ± 1.0		B7
J1709-4429	10	450	S	192	N	19.9	38.3	2	0.994	86.0 ± 1.3	-20.8 ± 0.9	A11
J1709-4429	20	2318	S	511	N	20.7	44.3	3	0.996	82.6 ± 0.4	-21.3 ± 0.3	A11
J1713-3949	10	2069	S	12	N	2.6	4.9		0.838			A11
J1713-3949	20	7776	S	26	N	6.5	11.8		0.957			A11
J1714-1054	20	960	S	34	N	4.2	7.7		0.986			B7
J1715-3903	10	569	S	17	N	13.7	25.0		0.855	55.5 ± 10.6		A11
J1715-3903	20	2165	S	21	N	14.7	26.9		0.791	56.3 ± 7.7		A11
J1717-5800	20	780	S	24	N	22.5	41.2		0.853			B7
J1718-3718	10	419	S	15	N	4.4	8.1		0.933			A11
J1718-3718	20	4835	S	22	Y	17.8	32.6		0.902			A11
J1718-3825	10	760	M	52	N	9.1	44.4		0.855	77.5 ± 3.9	-21.2 ± 2.9	A11
J1718-3825	20	3219	M	48	N	8.2	55.6		0.823	66.6 ± 3.1	-8.5 ± 2.0	A11
J1719-4006	20	960	S	48	N	11.1	20.2		0.962			B7
J1721-3532	10	419	M	364	N	12.2	24.2	3	0.941	32.3 ± 0.5	-9.6 ± 0.3	A11
J1721-3532	20	2135	S	219	Y	34.5	105.2	4	0.866	6.9 ± 0.9	-3.1 ± 0.5	A11
J1722-3632	20	719	D	78	N	5.7	31.6		0.818	14.8 ± 2.4	8.8 ± 1.6	B7
J1722-3712	10	580	S	47	N	4.9	11.1		0.969	31.5 ± 4.0	11.4 ± 2.8	A11
J1722-3712I	10	580	S	2	N	4.4	8.0		0.665			A12
J1722-3712	20	2136	S	177	N	5.8	12.8	2	0.987	42.4 ± 1.0	16.4 ± 0.7	A11
J1722-3712I	20	2136	S	18	N	7.5	13.7		0.925	52.7 ± 10.4		A12
J1723-3659	10	509	S	41	N	13.8	25.1		0.967	32.2 ± 4.6		A12
J1723-3659	20	2316	S	117	N	13.1	30.2	2	0.991	42.3 ± 1.7	-16.7 ± 1.2	A12
J1726-3530	10	1827	S	26	N	2.7	5.0		0.926	36.5 ± 7.1	-72.8 ± 4.9	A12
J1726-3530	20	9530	S	37	Y	12.2	34.5		0.890		-70.4 ± 3.5	A12
J1730-3350	10	700	S	95	N	5.0	12.0		0.986	65.3 ± 2.0	-5.7 ± 1.5	A12
J1730-3350	20	2437	S	145	Y	16.8	46.6	4	0.876	43.2 ± 1.6		A12
J1731-4744	10	538	M	368	N	7.9	10.7	3	0.932	13.8 ± 0.4		A12
J1731-4744	20	2754	M	2515	N	7.7	10.8	4	0.885	15.3 ± 0.1	5.2 ± 0.0	A12
J1733-2228	20	959	D	205	N	25.8	36.7	2	0.963	17.4 ± 0.7		B7
J1733-3716	10	629	D	95	N	4.6	51.7		0.791	60.2 ± 1.9	-11.9 ± 1.3	A12
J1733-3716	20	2406	D	162	N	5.4	59.9	4	0.835	64.5 ± 1.1	-11.9 ± 0.8	A12
J1734-3333	10	2288	D	37	N	7.7	32.4		0.850	48.5 ± 4.6	27.6 ± 3.4	A12
J1734-3333	20	11448	S	36	Y	43.6	153.7		0.814		18.2 ± 3.8	A12
J1735-3258	10	2259	S	41	N	9.7	23.7		0.943			A12
J1735-3258	20	19293	S	34	Y	79.6	164.3		0.777			A12
J1737-3137	10	1059	S	21	N	7.1	13.0		0.933	49.0 ± 8.7	35.9 ± 6.3	A12
J1737-3137	20	5968	S	59	N	11.7	30.0		0.943	40.0 ± 3.4	36.3 ± 2.3	A12
J1737-3555	20	959	S	66	N	6.5	11.9		0.992	20.0 ± 2.8		B7
J1738-2955	10	2379	S	10	N	6.7	12.2		0.782			A12
J1738-2955	20	10500	S	32	N	5.7	10.4		0.939	46.0 ± 5.7	-21.2 ± 4.0	A12
J1739+0612	20	960	S	40	N	13.8	25.1		0.986	16.2 ± 5.0		B8
J1739-1313	20	959	S	86	N	2.0	3.9		0.929	38.9 ± 1.9		B8

Table C1. continued.

Name	λ_{obs} [cm]	t_{obs} [sec]	Class	S/N	Scat.	W_{50} [$^{\circ}$]	W_{10} [$^{\circ}$]	N_{Comp}	Sym.	L [%]	V [%]	Fig.
J1739-2903	10	340	D	84	N	6.5	9.9		0.977			A13
J1739-2903I	10	340	S	21	N	7.9	14.4		0.891			A13
J1739-2903	20	2255	D	219	N	7.0	11.8	2	0.982		5.5 ± 0.9	A13
J1739-2903I	20	2255	S	101	N	8.0	15.3	2	0.975	19.5 ± 1.8	-3.9 ± 1.3	A13
J1739-3023	10	1000	S	14	N	11.2	20.4		0.873	48.9 ± 13.9		A13
J1739-3023	20	3248	S	55	N	10.8	19.8		0.979	61.0 ± 3.1	-9.7 ± 2.2	A13
J1740-3015	10	339	D	285	N	2.7	5.4	2	0.956	75.8 ± 0.6	-51.4 ± 0.4	A13
J1740-3015	20	2784	S	497	N	1.9	5.6	3	0.996	78.8 ± 0.3	-31.5 ± 0.2	A13
J1742-4616	20	659	S	43	N	20.2	36.9		0.970	21.1 ± 3.9	-14.6 ± 2.7	B8
J1743-3150	20	956	S	114	N	6.3	11.6	1	0.994	17.2 ± 1.7		B8
J1743-3153	20	1800	S	33	N	22.8	36.6		0.941		26.9 ± 4.6	B8
J1743-4212	20	1920	S	66	N	11.5	18.2		0.983	14.4 ± 1.4		B8
J1745-3040	10	449	M	207	N	8.0	23.7	4	0.927	42.6 ± 0.7		A13
J1745-3040	20	2253	M	865	N	6.2	20.7	6	0.897	43.7 ± 0.2		A13
J1749-3002	20	959	M	106	N	26.9	50.9	3	0.977	22.7 ± 1.7	10.7 ± 1.2	B8
J1750-3157	20	960	D	58	N	3.0	33.3		0.714	14.5 ± 3.5		B8
J1755-2534	20	1800	S	11	N	24.5	44.9		0.693			B8
J1756-2225	10	1168	D	15	N	14.2	17.8		0.835			A13
J1756-2225	20	4563	D	29	N	6.7	20.3		0.904			A13
J1757-2421	10	489	M	101	N	25.3	31.4	3	0.871	14.1 ± 1.5		A13
J1757-2421	20	2106	M	297	N	15.1	28.8	3	0.960	18.4 ± 0.5	2.9 ± 0.4	A13
J1759-2302	20	959	S	29	N	26.5	48.5		0.929			B8
J1801-2154	10	2709	S	14	N	7.9	14.4		0.915	40.5 ± 13.4		A13
J1801-2154	20	8554	S	27	N	8.7	15.8		0.965	34.8 ± 7.0		A13
J1801-2304	10	579	D	99	N	7.1	21.0		0.964	8.3 ± 2.0		A13
J1801-2304	20	2700	S	98	Y	63.1	197.7		0.760	10.2 ± 1.6	11.4 ± 1.1	A13
J1801-2451	10	700	S	19	N	10.8	19.8		0.911	51.2 ± 10.6		A13
J1801-2451	20	2468	S	79	N	13.0	23.7		0.984	62.9 ± 2.4	28.1 ± 1.6	A13
J1801-2920	20	959	M	127	N	16.9	19.8	3	0.955	31.5 ± 1.2	-8.4 ± 0.9	B8
J1803-2137	10	460	D	238	N	24.2	96.5	3	0.855	67.8 ± 0.8	35.4 ± 0.5	A14
J1803-2137	20	2587	M	341	N	35.3	116.9	3	0.940	51.8 ± 0.5	31.3 ± 0.3	A14
J1803-2712	20	960	S	43	N	18.4	33.6		0.973	38.2 ± 4.2		B8
J1805-0619	20	960	D	42	N	11.1	21.2		0.843	15.0 ± 4.1		B8
J1806-2125	10	1240	S	16	N	6.8	12.4		0.959			A14
J1806-2125	20	5973	S	43	Y	16.4	37.4		0.899		-11.0 ± 3.3	A14
J1808-0813	20	959	S	90	N	9.4	15.8		0.956	17.4 ± 2.0		B8
J1808-3249	20	959	D	88	N	3.5	17.6		0.817	20.6 ± 2.0	-7.5 ± 1.5	B8
J1809-0743	20	960	S	18	N	13.1	24.1		0.920			B8
J1809-1917	10	940	D	82	N	63.0	92.6		0.846	75.3 ± 2.2	36.4 ± 1.5	A14
J1809-1917	20	3848	D	72	N	75.2	102.9		0.850	69.4 ± 2.2	38.9 ± 1.4	A14
J1811-0154	20	959	S	39	N	7.8	15.1		0.919			B8
J1812-1910	10	2609	D	11	N	14.2	18.0		0.886			A14
J1812-1910	20	11125	S	26	N	22.1	40.4		0.929		38.6 ± 4.5	A14
J1814-1744	20	942	S	32	N	9.1	16.6		0.964			B8
J1815-1738	10	2230	S	21	N	4.9	8.9		0.948	76.7 ± 9.9		A14
J1815-1738	20	9277	S	37	Y	15.4	28.2		0.924	64.3 ± 5.1		A14
J1816-5643	20	960	S	11	N	10.3	18.8		0.955			B8
J1817-3837	20	959	S	114	N	4.6	9.5	2	0.897	11.9 ± 1.0		B8
J1819+1305	20	960	D	55	N	21.7	31.5		0.920			B9
J1820-1529	10	1999	S	40	N	5.9	10.7		0.985		11.8 ± 3.4	A14
J1820-1529	20	8285	S	57	Y	31.1	95.5		0.751		11.2 ± 2.8	A14
J1820-1818	20	960	S	62	N	15.1	27.0		0.929	13.8 ± 3.1		B9
J1821-1419	10	1987	S	6	N	11.4	20.8		0.561			A14
J1821-1419	20	8818	S	14	Y	29.1	53.3		0.818			A14
J1822-2256	20	958	S	181	N	9.2	15.9	2	0.992	19.8 ± 1.0	-3.7 ± 0.7	B9
J1824-1945	10	460	D	127	N	3.0	8.1	2	0.938	22.2 ± 1.4	-7.9 ± 0.9	A14
J1824-1945	20	3695	S	1055	N	3.1	5.9	3	0.994	17.4 ± 0.2	0.5 ± 0.1	A14
J1825-1446	10	419	S	124	N	4.1	10.4	2	0.958	55.9 ± 1.5	-3.9 ± 1.0	A14
J1825-1446	20	2496	S	175	Y	11.9	28.4	2	0.948	54.5 ± 1.1		A14
J1826-1334	10	420	D	88	N	15.6	105.9		0.815	67.9 ± 2.1	36.7 ± 1.6	A14
J1826-1334	20	2528	D	168	N	21.6	123.6	3	0.854	71.9 ± 1.2	37.2 ± 0.8	A14
J1828-1057	10	2509	S	20	N	20.5	37.5		0.891			A15
J1828-1057	20	14524	S	30	N	22.5	41.1		0.971		-14.7 ± 3.7	A15
J1828-1101	10	570	S	90	N	4.8	9.7		0.991	50.4 ± 2.8		A15

Table C1. continued.

Name	λ_{obs} [cm]	t_{obs} [sec]	Class	S/N	Scat.	W_{50} [°]	W_{10} [°]	N_{Comp}	Sym.	L [%]	V [%]	Fig.
J1828-1101I	10	570	S	23	N	7.4	13.6		0.955	52.9 ± 9.2	-26.7 ± 6.2	A15
J1828-1101	20	2738	S	57	Y	34.1	104.2		0.796	60.0 ± 2.7	20.2 ± 1.7	A15
J1828-1101I	20	2738	S	12	Y	36.6	67.6		0.850		-25.5 ± 6.6	A15
J1830-1059	10	689	M	60	N	2.0	6.7		0.986	65.6 ± 3.3	-24.8 ± 2.3	A15
J1830-1059	20	6333	S	156	N	2.4	7.1	3	0.990	80.1 ± 1.1	-15.4 ± 0.8	A15
J1831-0952	10	900	D	15	N	41.8	59.0		0.780	49.3 ± 9.3		A15
J1831-0952	20	11219	S	37	N	44.1	71.3		0.860	61.3 ± 4.1	-20.1 ± 3.1	A15
J1832-0827	10	448	D	93	N	2.2	11.7		0.946	12.3 ± 1.9		A15
J1832-0827	20	2428	D	280	N	2.6	12.1	3	0.936	20.1 ± 0.6		A15
J1833-0827	10	570	M	82	N	22.8	59.7		0.874	34.4 ± 2.2		A15
J1833-0827	20	2229	M	188	N	10.0	37.7	3	0.966	6.5 ± 0.9	2.8 ± 0.7	A15
J1834-0731	10	869	S	28	N	8.6	15.9		0.991			A15
J1834-0731	20	3510	S	52	Y	20.1	66.2		0.832	14.7 ± 3.3	16.5 ± 2.3	A15
J1835-0643	10	480	D	22	N	7.4	19.3		0.811			A15
J1835-0643	20	2645	S	73	Y	37.1	114.3		0.809			A15
J1835-0944	10	900	S	16	N	12.5	22.7		0.920			A15
J1835-0944	20	3329	S	37	N	18.3	33.5		0.966			A15
J1835-1106	10	450	S	34	N	8.3	15.2		0.975	47.6 ± 5.3		A15
J1835-1106	20	2138	S	150	N	8.5	18.6	2	0.993	51.7 ± 1.2	10.2 ± 0.8	A15
J1837+1221	20	956	D	37	N	2.3	8.4		0.885	17.0 ± 4.6		B9
J1837-0045	20	960	S	25	N	7.3	13.3		0.976			B9
J1837-0559	10	1409	S	19	N	8.5	15.8		0.984			A16
J1837-0559	20	3817	S	31	N	16.5	30.1		0.941			A16
J1837-0604	10	1950	S	57	N	8.6	15.7		0.986	77.3 ± 4.4		A16
J1837-0604	20	9948	S	41	Y	46.1	109.7		0.837	33.2 ± 4.7		A16
J1837-1837	20	960	S	31	N	5.5	10.2		0.978	21.1 ± 5.9		B9
J1838-0453	10	1619	S	12	N	7.0	12.6		0.926			A16
J1838-0453	20	4943	S	37	N	11.9	21.8		0.931	28.7 ± 4.8		A16
J1838-0549	10	2129	D	15	N	5.8	22.4		0.818			A16
J1838-0549	20	3597	S	24	N	10.6	19.3		0.942			A16
J1839-0321	10	1649	S	11	N	4.6	8.6		0.931			A16
J1839-0321	20	4317	S	27	N	9.6	17.6		0.942			A16
J1839-0905	10	3809	D	22	N	11.7	14.3		0.931			A16
J1839-0905	20	15663	D	42	N	14.4	20.6		0.887			A16
J1841-0345	20	1830	S	64	N	19.3	35.4		0.980	83.0 ± 3.3		B9
J1841-0425	10	509	S	60	N	8.2	14.7		0.983	47.8 ± 3.4		A16
J1841-0425	20	1957	S	213	N	8.5	14.6	2	0.994	58.9 ± 0.9		A16
J1841-0524	10	2369	S	9	N	5.4	10.2		0.917			A16
J1841-0524	20	12360	S	27	N	10.8	19.7		0.966		-17.4 ± 4.0	A16
J1841-7845	20	900	S	15	N	22.5	41.1		0.836			B9
J1842+1332	20	960	S	25	N	63.5	119.4		0.958			B9
J1842-0905	10	749	D	24	N	13.2	20.9		0.826			A16
J1842-0905	20	2434	D	81	N	6.3	20.6		0.873			A16
J1843-0355	10	1650	D	39	N	31.2	43.8		0.982	34.7 ± 4.8	22.9 ± 3.4	A16
J1843-0355	20	7268	S	30	Y	50.9	94.7		0.911		20.1 ± 3.7	A16
J1843-0702	20	6186	S	32	N	7.0	12.8		0.985		18.2 ± 4.4	B9
J1843-0702I	20	6186	S	17	N	10.8	19.8		0.879			B9
J1844-0256	10	2159	S	29	N	26.1	47.9		0.957	44.4 ± 6.7	-21.4 ± 5.3	A17
J1844-0256	20	12605	S	35	Y	62.7	118.1		0.870		-12.8 ± 3.5	A17
J1844-0538	10	520	S	48	N	5.8	13.4		0.966	35.1 ± 4.3		A17
J1844-0538	20	1866	S	185	N	10.0	21.1	2	0.982	43.6 ± 1.0	10.8 ± 0.8	A17
J1845-0316	20	1799	S	24	N	18.7	34.2		0.810		24.8 ± 6.2	B9
J1845-0434	10	580	M	114	N	10.1	14.7	2	0.932	13.3 ± 1.5	-4.3 ± 1.1	A17
J1845-0434	20	2042	D	188	N	11.8	16.8	2	0.969	14.9 ± 0.9	-5.0 ± 0.6	A17
J1845-0743	10	460	M	53	N	14.0	31.6		0.864	19.3 ± 3.4		A17
J1845-0743	20	2588	M	181	N	7.1	31.7	4	0.912	15.2 ± 0.8	3.1 ± 0.6	A17
J1847-0402	10	459	D	102	N	4.4	15.7	3	0.934	31.7 ± 1.7	5.6 ± 1.2	A17
J1847-0402	20	1772	M	299	N	12.1	17.6	3	0.858	17.7 ± 0.5	5.4 ± 0.4	A17
J1848-1414	20	960	S	26	N	15.1	27.5		0.925		28.1 ± 4.9	B9
J1852-2610	20	1919	D	88	N	9.7	30.2		0.940	26.7 ± 2.0		B9
J1853+0011	20	5998	S	23	N	9.1	16.5		0.969			B9
J1853-0004	10	1050	S	23	N	3.6	6.7		0.952	79.0 ± 9.4		A17
J1853-0004	20	2309	D	38	N	6.7	43.1		0.833	70.6 ± 7.0		A17
J1855-0941	20	960	S	33	N	21.0	46.9		0.862			B9

Table C1. continued.

Name	λ_{obs} [cm]	t_{obs} [sec]	Class	S/N	Scat.	W_{50} [°]	W_{10} [°]	N_{Comp}	Sym.	L [%]	V [%]	Fig.
J1901-0906	20	898	D	228	N	9.0	11.3	4	0.952	28.4 ± 0.8		B9
J1901-1740	20	957	S	12	N	9.7	17.8		0.933			B9
J1904+0004	20	960	S	104	N	19.1	34.9	1	0.983	23.9 ± 1.6	14.4 ± 1.2	B9
J1904-1224	20	959	S	26	N	3.2	11.2		0.821			B9
J1919+0134	20	959	D	105	N	9.6	17.9	2	0.927	19.3 ± 1.6	-8.9 ± 1.1	B10
J1932-3655	20	959	D	51	N	3.8	13.0		0.959	27.0 ± 3.4	11.1 ± 2.4	B10
J1943+0609	20	960	D	37	N	7.2	16.7		0.823			B10
J1944-1750	20	1918	S	24	N	20.9	38.4		0.958			B10
J1946-1312	20	959	S	24	N	7.9	14.6		0.966			B10
J1946-2913	20	959	S	49	N	3.9	10.9		0.904			B10
J1947+0915	20	657	S	13	N	7.4	13.5		0.938			B10
J1949-2524	20	959	S	3	N	2.7	5.2		0.949			B10
J1956+0838	20	959	S	34	N	16.3	29.8		0.983			B10
J2006-0807	20	1919	M	210	N	48.2	64.7	3	0.989	37.0 ± 0.8		B10
J2007+0809	20	960	S	21	N	88.0	172.2		0.915			B10
J2048-1616	20	957	M	1915	N	12.1	15.1	3	0.833	37.5 ± 0.1	3.8 ± 0.0	B10
J2108-3429	20	1918	S	70	N	3.7	6.7		0.974	8.5 ± 2.8	19.7 ± 2.0	B10
J2116+1414	20	960	S	45	N	7.1	20.3		0.957			B10
J2248-0101	20	959	S	32	N	6.9	12.5		0.985			B10
J2346-0609	20	958	D	55	N	15.3	18.3		0.964	33.7 ± 3.0	10.1 ± 1.9	B10

Table C1. continued.